https://doi.org/10.5194/acp-2022-504
Preprint. Discussion started: 18 July 2022

Atmospheric Chemistry and Physics Discussions

Diurnal variability of atmospheric O_2, CO_2 and their exchange ratio above a boreal forest in southern Finland

Kim A.P. Faassen[1], Linh N.T. Nguyen[2], Eadin R. Broekema[2], Bert A.M. Kers[2], Ivan Mammarella[3], Timo Vesala[3,4], Penelope A. Pickers[5], Andrew C. Manning[5], Jordi Vilà-Guerau de Arellano[1,6], Harro A.J. Meijer[2], Wouter Peters[1,2], and Ingrid T. Luijkx[1]

[1]Meteorology and Air Quality, Wageningen University and Research, Wageningen, the Netherlands
[2]Centre for Isotope Research (CIO), Energy and Sustainability Research Institute Groningen, University of Groningen, Groningen, the Netherlands
[3]Institute for Atmospheric and Earth System Research (INAR) / Physics, Faculty of Science, University of Helsinki, Helsinki, Finland
[4]INAR/Forest Sciences, Faculty of Agriculture and Forestry, University of Helsinki, Helsinki, Finland
[5]Centre for Ocean and Atmospheric Sciences, School of Environmental Sciences, University of East Anglia, Norwich, NR4 7TJ, United Kingdom
[6]Atmospheric Chemistry Department, Max Planck Institute for Chemistry, 55128 Mainz, Germany

Correspondence: Kim A.P. Faassen (kim.faassen@wur.nl)

Abstract. The exchange ratio (ER) between atmospheric O_2 and CO_2 is a useful tracer on global and local scales to better understand the carbon budget. The variability of ER (in mol O_2 per mol CO_2) between terrestrial ecosystems is not well-known, and there is no consensus on how to derive the ER signal to represent an ecosystem, as there are different approaches available, either based on concentration (ER_{atmos}) or flux measurements (ER_{forest}). In this study we measured atmospheric O_2 and CO_2 concentrations at two heights above the boreal forest in Hyytiälä, Finland. Such measurements of O_2 are unique and enable us to potentially identify which forest carbon loss and production mechanisms dominate over various hours of the day. We found that the ER_{atmos} signal at 23 m is not representative for the forest exchange alone but is also influenced by other factors, including for example entrainment of air masses with different thermodynamic and atmospheric composition characteristics in the atmospheric boundary layer. To derive ER_{forest} we infer O_2 fluxes using multiple theoretical and observation-based micro-meteorological formulations to determine the most suitable approach. Our resulting ER_{forest} shows a distinct difference in behaviour between daytime (0.92 $\pm$ 0.17 mol/mol) and nighttime (1.03 $\pm$ 0.05 mol/mol). These insights demonstrate the diurnal variability of different ER signals above a boreal forest and we also confirmed that the signals of ER_{atmos} and ER_{forest} can not be used interchangeably. Therefore, we recommend measurements on multiple vertical levels to derive O_2 and CO_2 fluxes for the ER_{forest} signal, instead of a single level time series of the concentrations for the ER_{atmos} signal. We show that ER_{forest} can be further split into specific signals for respiration (1.03 $\pm$ 0.05 mol/mol) and photosynthesis (0.96 $\pm$ 0.12 mol/mol). This estimation allows us to separate the Net Ecosystem Exchange (NEE) into Gross Primary Production (GPP) and Total Ecosystem Respiration (TER), giving comparable results to the more commonly used eddy covariance approach. Our study shows the potential of using atmospheric O_2 as an alternative method to gain new insights on the different CO_2 signals that contribute to the forest carbon budget.

https://doi.org/10.5194/acp-2022-504
Preprint. Discussion started: 18 July 2022

Atmospheric Chemistry and Physics Discussions

1 Introduction

To understand how the increasing carbon dioxide (CO_2) levels in the atmosphere are changing our climate, we need to know the sources and sinks of CO_2 separately. These sources and sinks result in the global carbon budget in which the main sources are fossil fuel combustion and land-use change and the main sinks are the uptake by the land biosphere and the oceans (Friedlingstein et al., 2022). The net terrestrial biospheric sink (Net Ecosystem Exchange, NEE) results from many fluxes of which the two largest are typically Gross Primary Production (GPP) and the Total Ecosystem Respiration (TER). Knowing these gross fluxes separately will allow better estimates of the changing behaviour of the biosphere carbon sink, as GPP and TER respond differently to climate change and increasing atmospheric CO_2 levels.

Using additional tracers allows us to gain further insights into GPP and TER, without relying on a temperature-based function to parameterize TER as is used for Eddy Covariance (EC) measurements e.g. Reichstein et al. (2005). Additional tracers such as atmospheric O_2 (Keeling and Manning, 2014), and also COS, $\delta^{13}C$ or $\Delta^{17}O$ have the important advantage of sharing a process or pathway with CO_2 directly (Whelan et al., 2018; Peters et al., 2018; Koren et al., 2019; Kooijmans et al., 2021). This allows one to use numerical models to test formulations of processes, such as stomatal and mesophyl exchange, photosynthesis, pool-specific respiration, and even turbulent canopy exchange. Atmospheric O_2 is directly coupled to CO_2 in several processes through the so-called Exchange Ratio (ER) (Keeling and Manning, 2014; Manning and Keeling, 2006; Keeling et al., 1993). This ER (also sometimes referred to as Oxidative Ratio (OR) in the literature), indicates the amount of moles of O_2 that are exchanged per mole of CO_2 and gives a process-specific signature (Keeling, 1988).

On the global scale, ER has been used to derive the global oceanic CO_2 sink and determine the global carbon budget (Stephens et al., 1998; Rödenbeck et al., 2008; Tohjima et al., 2019). This is done by solving the atmospheric budgets of O_2 and CO_2 with the following equations:

$$\frac{dCO_2}{dt} = F - O - B \tag{1}$$

$$\frac{dO_2}{dt} = -\alpha_F F + \alpha_B B + Z_{O_2} \tag{2}$$

where F is the fossil fuel CO_2 emissions, O is ocean CO_2 uptake, B is the net land biosphere sink of CO_2 and Z_{O_2} indicates the ocean O_2 outgassing. α_F and α_B indicate the ERs for fossil fuel combustion and the net land biosphere sink respectively. In these global studies simplified global average values ares used for α_F and α_B, where α_F is determined by the global mixture of fuels burned, which results in 1.38 [mol/mol] (Keeling and Manning, 2014) and α_B was determined by laboratory measurements and a literature study of ORs of different plant and soil materials, which resulted in 1.1 [mol/mol] (Severinghaus, 1995). Furthermore, α_B is also used to combine O_2 and CO_2 into Atmospheric Potential Oxygen (APO) (Stephens et al., 1998) which is used in determining the ocean carbon sink, and recently has also been shown to be a suitable tracer to detect fossil fuel emission reductions during the COVID-19 pandemic (Pickers et al., 2022). For these larger scale applications using APO

https://doi.org/10.5194/acp-2022-504
Preprint. Discussion started: 18 July 2022


Atmospheric Chemistry and Physics Discussions

it is important to have good estimates for α_B.

On local scales, previous studies have shown that α_B is not a constant value as used on the global scale, and that it shows a certain degree of temporal and spatial variability. These studies either measured ORs from elemental composition analysis (Worrall et al., 2013; Randerson et al., 2006; Gallagher et al., 2017), or derived the ER from atmospheric concentrations measurements (Battle et al., 2019; Seibt et al., 2004; van der Laan et al., 2014). By using elemental composition analysis, the OR reflects the relationship between O_2 and CO_2 over a longer time scale, of years or decades, compared to the atmospheric concentration measurements of the ER, which are on hourly and daily time scales. Both the OR and the ER based studies showed that α_B changes per ecosystem and over different time periods. The ER from the gas exchange experiments can furthermore be used for the separation of GPP and TER, using a specific ecosystem ER, which are determined with two alternative approaches (see Figure 1) (Seibt et al., 2004; Stephens et al., 2007; Ishidoya et al., 2013, 2015; Battle et al., 2019). The first is the ER of the atmosphere (ER_{atmos}), which is the ratio of the atmospheric O_2 and CO_2 concentration measurements, and the second is the ER of the forest (ER_{forest}), which is the ratio of the surface fluxes of O_2 and CO_2. First attempts to estimate ER_{forest} were made using one-box models (Seibt et al., 2004; Ishidoya et al., 2013). More accurate estimates of ER_{forest} would be based on in-situ measured O_2 and CO_2 surface fluxes, however O_2 currently cannot yet be measured accurately using EC techniques. Ishidoya et al. (2015) showed the first surface fluxes of O_2 using vertical gradients of O_2, an alternative technique to EC, and CO_2 measurements at two heights above the canopy in the surface layer in a temperate forest in Japan. Their results showed that the ER_{forest} signal could be used to separate the NEE signal into GPP and TER, consistent with the separation method for EC measurements using an empirical function of air temperature.

When using O_2 to separately estimate GPP and TER fluxes, it is important to use the value for ER that represents ecosystem exchange. Seibt et al. (2004) showed that the signal of ER_{atmos} cannot be directly linked to the exchange of carbon in the terrestrial biosphere, because in addition to the biosphere, ER_{atmos} is also affected by advection, boundary layer dynamics and entrainment (Figure 1). In contrast, Ishidoya et al. (2015) found similar values for ER_{atmos} and ER_{forest}. So far, there is no clear consensus on which signal should be used to indicate the ER of the ecosystem. Furthermore, since atmospheric O_2 measurements are challenging to make, only a few studies exist that measured atmospheric O_2 continuously above an ecosystem and that derive ER signals (Ishidoya et al., 2015; Stephens et al., 2007; Seibt et al., 2004; Battle et al., 2019). The uncertainty and spatial and temporal variability of α_B are therefore not well known (Manning and Keeling, 2006; Keeling and Manning, 2014), and knowledge about the difference between ER_{forest} and ER_{atmos}, its variability across difference regions and ecosystems, and how ER_{forest} can be used on both the local and global scale to advance our understanding of the carbon cycle, is still limited. Therefore, more and longer in-situ time series of atmospheric O_2 measurements are needed and further understanding of O_2 and CO_2 exchange above and below the canopy is crucial to continue the pioneering work of Seibt et al. (2004), Stephens et al. (2007), Ishidoya et al. (2015) and Battle et al. (2019) and improve the application of the global biosphere ER, resulting in a better understanding of the carbon balance on local, regional and global scales.

https://doi.org/10.5194/acp-2022-504
Preprint. Discussion started: 18 July 2022

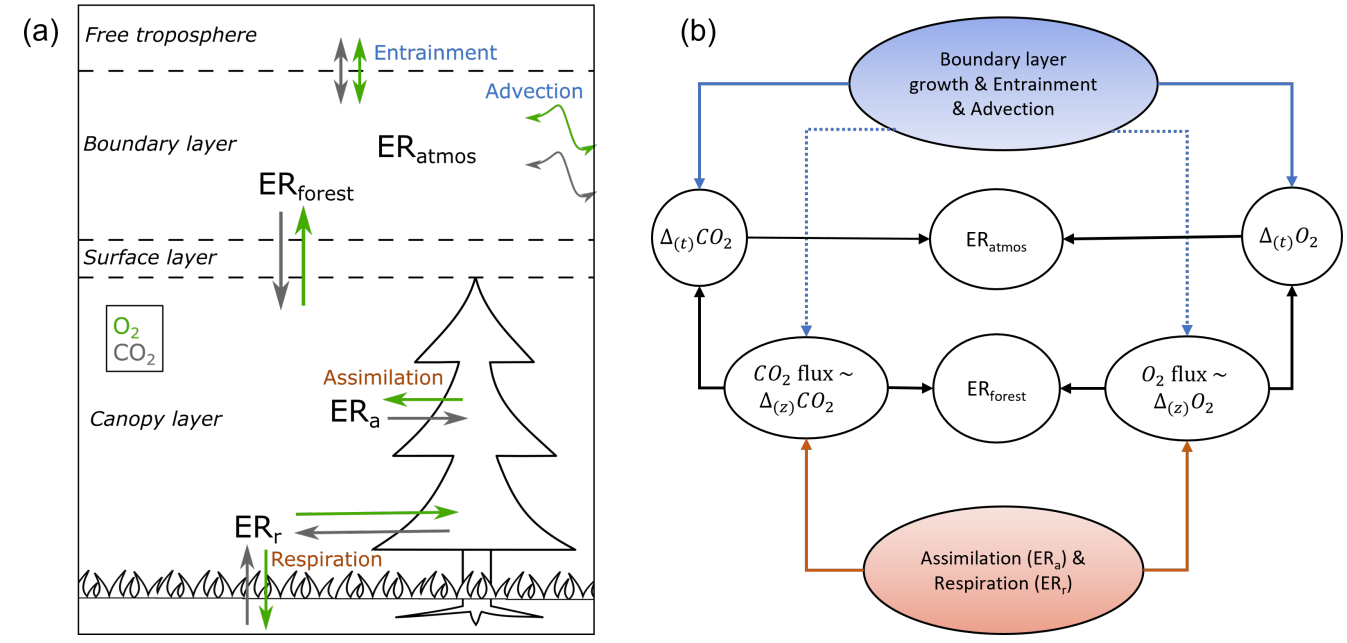

Figure 1. Schematic overview of the different O_2:CO_2 exchange ratio signals (ER), measured and analyzed in and above a forest, influenced by the different O_2 and CO_2 fluxes and meteorological processes (a), together with a more detailed look on which processes influence the different ER signals (b). (a) shows the direction of the surface fluxes during the day in the surface layer, which includes the roughness sublayer and the inertial sublayer. During the night the direction of the O_2 and the CO_2 surface fluxes are the other way around. The ER of the atmosphere (ER_{atmos}) is determined from the change over time ($\Delta_{(t)}$) in the O_2 and CO_2 concentration measurements, and the ER of the forest (ER_{forest}) is calculated from the surface fluxes of O_2 and CO_2 which are inferred ($\sim$) from the vertical gradient ($\Delta_{(z)}$). ER_a represents assimilation processes and ER_r represents respiration processes. (b) shows the connections between the processes, measurements, and the ERs. Dotted lines indicates smaller influences of the processes that are connected to it compared to solid lines.

The aim of this study is to improve upon existing methods to calculate ER_{forest} and get a better comparison between how the ER_{atmos} and ER_{forest} signals are formed. We carried out a measurement campaign in Hyytiälä, Finland, for two short periods in spring/summer 2018 and 2019 where both O_2 and CO_2 were measured at two heights with a setup including a differential fuel cell analyser for O_2. These new measurements extend the existing continuous O_2 records and provide us the opportunity to calculate the O_2 surface fluxes in a boreal forest for the first time, together with the CO_2 surface flux. We used our measurements to determine the relation between O_2 and CO_2 diurnal behaviour of the concentrations and the fluxes, by using either one or both measurement heights on the tower. Combining the O_2 and the CO_2 fluxes allowed us to calculate ER_{forest}, make a comparison between the ER_{atmos} and ER_{forest} signals, and use ER_{forest} to estimate GPP and TER fluxes.

In this paper, we first describe the measurement site, experimental setup and methods to derive O_2 fluxes and the different ER signals (Section 2). We present the measurements for the whole campaign and select a representative day to determine the

https://doi.org/10.5194/acp-2022-504
Preprint. Discussion started: 18 July 2022


Atmospheric Chemistry and Physics Discussions

most suitable approach for deriving O_2 fluxes and to determine ER_{forest} (Section 3). A detailed evaluation and discussion of our ER_{atmos} and ER_{forest} signals is given in Section 4. We finalize with our conclusion about the diurnal variability of the ER signals for a representative day of a boreal forest (Section 5).

2 Methods

To determine ER_{atmos} and ER_{forest}, and its diurnal variability, we measured O_2 and CO_2 continuously at two heights above a boreal forest during two short campaigns at Hyytiälä. These 'OXHYYGEN' (OXYGEN at HYYtiälä) campaigns took place in the spring/summer of 2018 (03-Jun through 02-Aug) and 2019 (10-Jun through 17-Jul). In this section, we describe the measurement site and instrumental setup, as well as the methods used to determine the O_2 and CO_2 fluxes from the measured vertical gradient and the ER signals.

2.1 Measurement site

The measurements were made at Hyytiälä SMEAR II Forestry Station of the University of Helsinki in Finland (61° 51'N, 24°17' E, +181 MSL); this site is described in more detail in e.g. Hari et al. (2013). The SMEAR II station is a boreal site within the European Integrated Carbon Observation System (ICOS) network with atmospheric and ecosystem measurements. The SMEAR II station is located inside a homogeneous forest of Scots pine trees (*Pinus Sylvestris*) with a dominant canopy height of 18 m and some silver birch and aspen trees. The forest floor is covered with mosses and herbs. The soils are podzols on top of glacial till. A large lake is located close to the measurement site and has a fetch of 250 m over the dominant wind direction of 230°. The footprint of the site is mostly influenced by natural sources, with the atmospheric signal dominated by forest exchange (Carbon Portal ICOS RI, 2022). The measurement site includes several towers, including a 128m tall tower and a 23 m high walk up tower, where atmospheric variables and gas concentrations are continuously measured. The operational data from this tower are publicly available online at http://avaa.tdata.fi/web/smart/smear/. Our O_2 and CO_2 measurement setup was installed in a cabin at the bottom of the 23 m high tower, and air was sampled from aspirated inlets (Blaine et al., 2006), installed at 23 m in the smaller tower and at 125 m in the tall tower, 5m and 107m above the canopy height respectively. We used both levels to calculate the vertical gradient for the flux calculations (Section 2.3).

2.2 Experimental setup

The measurement setup is based on the instrument used in van Leeuwen and Meijer (2015), following the methods in van der Laan-Luijkx et al. (2010) and Stephens et al. (2007). O_2 is measured with a Sable Systems "Oxzilla II" fuel cell based instrument and CO_2 is measured with an ABB continuous gas analyzer "URAS26", which is a non-dispersive infrared (NDIR) photometer. The gas handling schematic is shown in Figure 2.

https://doi.org/10.5194/acp-2022-504
Preprint. Discussion started: 18 July 2022

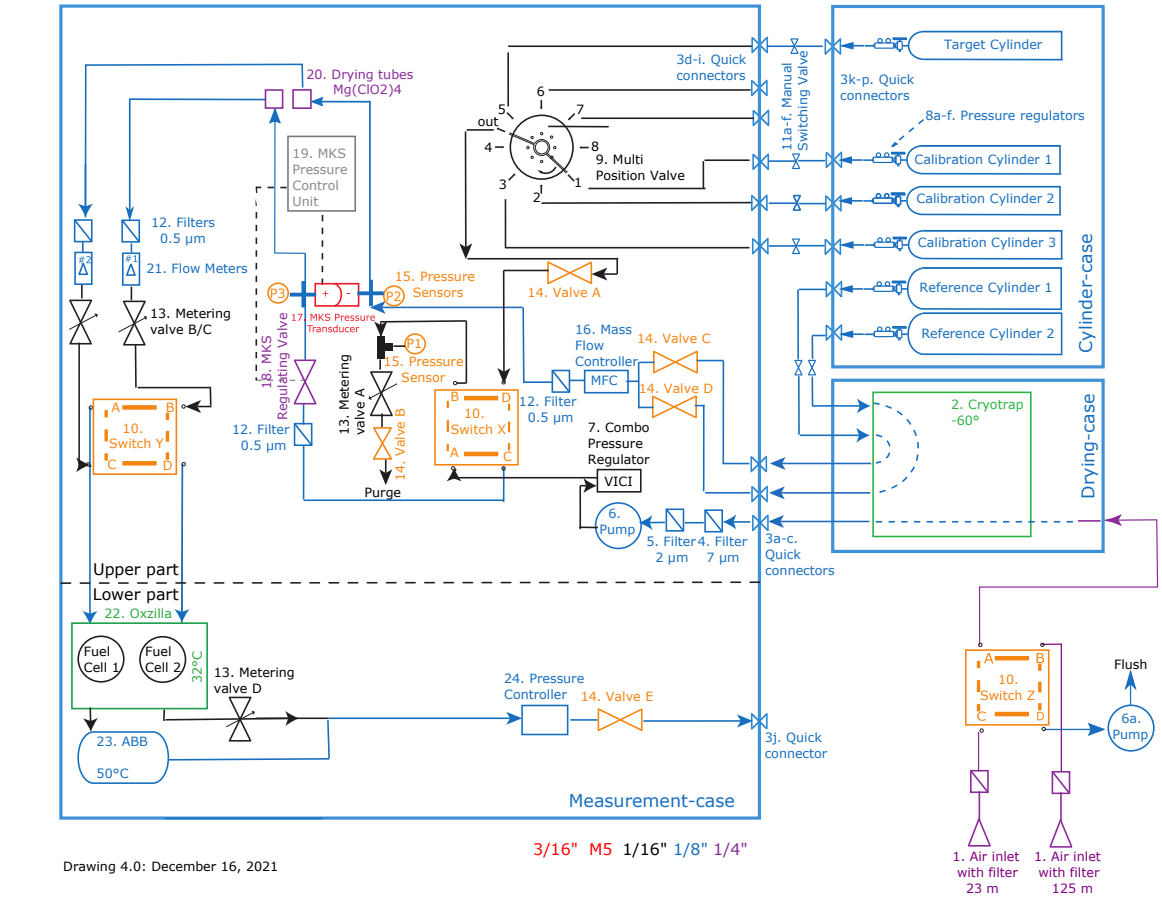

Figure 2. Schematic overview of the measurement setup used at Hyytiälä. The setup includes an Oxzilla O_2 fuel cell analyser and a URAS26 NDIR CO_2 analyser. The system measured air sampled from two heights of either 23 or 125 meters.

Air was pumped from either 23 or 125 metre height to the measurement system at the base of the tower. Both inlet lines were continuously flushed, where either one of the heights is measured by the system with a sample flow of around 120 ml/min and the other flushed to the room with a higher flow rate of around 2 litre per minute, which allows fast switching between the two heights. We switched between the inlets every half hour to match the Eddy Covariance (EC) measurements and to get a more stable signal of O_2. The air of the selected inlet was first cooled to -60 °C with a cryogenic cooler to remove water vapour from the air, before entering the system. Second stage drying of the air streams is done with magnesium perchlorate ($Mg(ClO_4)_2$) traps. The sample air was continuously measured against a reference gas (differentially for O_2, and alternatively for CO_2), and the pressure in both sample and reference line were matched to be the same using a pressure control system (MKS Instruments, types 223B, 248A and 250E for the pressure transducers, regulating valve and control system respectively). The reference and sample lines were switched every 2 minutes between the two fuel cells in the Oxzilla analyser. We measured a set of 3

https://doi.org/10.5194/acp-2022-504
Preprint. Discussion started: 18 July 2022


Atmospheric Chemistry and Physics Discussions

calibration cylinder and 1 target cylinder every 23 hours for half an hour per cylinder.

The measurements of these calibration gases allowed calibration of our measurements against the international Scripps Institution of Oceanography (SIO) scale for $\delta O_2/N_2$. We did that by using cylinders that are filled in the laboratory at the University of Groningen, where they were calibrated with the primary Scripps cylinders (Nguyen et al., 2022). The O_2 measurements are normally expressed as $\delta O_2/N_2$ ratios in 'per meg' units instead of mole fraction (ppm), since O_2 is not a trace gas because of its high abundance of 20.95%, and therefore the mole fraction varies due to changes of other gases, such as CO_2 (Keeling et al., 1998). $\delta O_2/N_2$ is defined as:

$$\delta(O_2/N_2) = \left(\frac{(O_2/N_2)_{\text{sample}}}{(O_2/N_2)_{\text{reference}}} - 1 \right) \cdot 10^6 \text{ [per meg]} \quad (3)$$

For simplicity, in this paper we use the term O_2 instead of $\delta O_2/N_2$, and we use the term 'concentration' rather than 'mole fraction' when discussing both CO_2 and O_2. Equation 3 indicates a change compared to a reference level. Negative values therefore indicate concentrations of O_2 lower than the reference value. To allow comparison of changes in CO_2 and O_2 directly, we converted the units of O_2 from per meg to ppm equivalents (ppmEq), where a change of 1 ppm CO_2 corresponds to a 4.77 per meg change in O_2 (Tohjima et al., 2005; Kozlova and Manning, 2009).

We modified the method described in van der Laan-Luijkx et al. (2010), to calibrate the measurements. The raw CO_2 measurements have a frequency of one measurement per six second, the raw O_2 measurements have a frequency of one measurement per second and both give 1 value every 4 minutes in the form of ΔCO_2 and $\Delta(\Delta)O_2$ respectively. CO_2 is measured on a single cell instrument, and therefore ΔCO_2 is the difference between the 2-minute averages of the sample air (S) and the reference cylinder (R), giving (S-R). For the 2-minute averaged CO_2 measurements, the last 78 seconds of each 2 minute period are used. Note that for CO_2, the NDIR system is different compared to other systems used and therefore does not need a zero-gas (Pickers et al., 2017). O_2 is measured on a double cell instrument, and therefore gives a double differential signal. The $\Delta(\Delta)O_2$ is the difference between the 2-minute averaged difference between S and R and the 2-minute averaged difference between R and S ((S-R)-(R-S)). For the 2-minute averaged O_2 values, the last 100 seconds of each 2 minute period are used. In 2019, the pressure control valve was not functioning optimally. We therefore corrected the 4-minute values of $\Delta(\Delta)O_2$ for a deviation in the MKS pressure sensor (PMKS), by multiplying $\Delta(\Delta)O_2$ with 0.095*PMKS, which we derived based on the measurements of the calibration cylinders. For both CO_2 and O_2, the 4-minute values were subsequently used to calculate half hourly means, where we excluded the first 4-minute value after the heights are switched, together with the measurements that did not fall inside the boundary based on the median absolute deviation (MAD) (Rousseeuw and Verboven, 2002).

The linear calibration response functions for both O_2 and CO_2 were calculated for every measurement period of the calibration cylinders, which was about every 23 hours. For the response functions, we used a constant slope based on the mean of all the calibration slopes measured in the specific year. The y-intercept of the response functions were interpolated to the time of the measurement, based on the two calibrations bracketing the measurement time. To facilitate the comparison of the O_2 and

https://doi.org/10.5194/acp-2022-504
Preprint. Discussion started: 18 July 2022

Atmospheric Chemistry and Physics Discussions

CO_2 measurements of the two heights and allow flux calculations based on the vertical gradient, we interpolated the data to one measurement for every 30 minutes for each height. Based on the target cylinders, measured during the calibration period, the stability of the long-term measurements were determined (Table 1). A different target cylinder for 2019 compared to 2018 was used, which resulted in different outcomes for the standard deviation (std) and the mean difference for these periods. The mean difference is determined by calculating the mean of the difference between the values of the target cylinder based on our own calibration and based on the declared value with calibration in Groningen. The measurement period of 2018 was also longer and therefore more points were included for the std and mean difference calculations. The measurement precision of this device compared to the recommendations of the World Meteorological Organisation (WMO) will be further discussed in section 4.1.

Table 1. The mean difference and the standard deviation (std) of the target cylinder measurements of O_2 and CO_2 for the 2018 and 2019 periods separately, together with the amount of data points used to calculated these specific values.

	2018 (03-06 through 01-08)			**2019** (16-06 through 17-07)		
	Std	Mean difference	Amount of points	Std	Mean difference	Amount of points
O_2 [per meg]	16	28	53	19	22	22
CO_2 [ppm]	0.07	0.7	53	0.07	0.5	22

2.3 Data analysis

For the analyses presented in this paper we needed representative diurnal cycles of O_2 and CO_2. We looked for a representative day in 2019 where little to no clouds were present, no unexpected behaviour in the diurnal cycles for potential temperature, specific humidity and CO_2 occurred, for example caused by advection, and where the O_2 data showed a clear difference between the two measurement heights. We used data from 2019 instead of 2018 because 2018 saw a large-scale drought in Europe, and 2019 was less extreme and closer to a typical boreal summer (Peters et al., 2020). However, no single representative day could be found in our 2019 record, where the O_2 data showed a clear negative vertical gradient during the day and positive during the night, in combination with the above-mentioned meteorological criteria. We therefore choose a sequence of days to create an aggregate day based on the average of several days, which is representative for this time of the year in Hyytiälä, following the same method used by Ishidoya et al. (2015). The main criterion was that the O_2 gradient had to be negative during the day and the negative relationship between O_2 and CO_2 concentrations at 23 m was present during the entire day. This resulted in selecting the period of 7 through 12 July 2019 to create the representative day which we used in all subsequent analyses.

For the representative day, the two O_2 : CO_2 Exchange Ratio (ER) signals, ER_{atmos} and ER_{forest}, were determined. ER_{atmos} is expressed as:

$$ER_{atmos} = -\frac{\Delta_{(t)}O_2}{\Delta_{(t)}CO_2} \tag{4}$$

https://doi.org/10.5194/acp-2022-504
Preprint. Discussion started: 18 July 2022

Atmospheric Chemistry and Physics Discussions

Where both $\Delta_{(t)}O_2$ and $\Delta_{(t)}CO_2$ are the change in concentration over a selected time period (t). This is a unit-less quantity as it represents mol O_2 per mol CO_2. ER_{atmos} was determined by the slope between the concentration of O_2 and CO_2 at the same height over a specific time period (Seibt et al., 2004; Stephens et al., 2007; Ishidoya et al., 2013; Battle et al., 2019). The selected time periods were based on the period when O_2 and CO_2 had the highest negative correlation. Throughout the day, this could be divided into three periods when different processes dominate (Figure 1). It starts with the period during the night where the atmosphere is stable and respiration becomes the dominant surface flux (P1), and therefore the CO_2 concentration increases and the O_2 concentration decreases. Subsequently, when the sun starts to rise, the boundary layer height starts to grow and entrainment of air from the free troposphere influences the surface measurements (P2) (Vilà-Guerau de Arellano et al., 2004). Here the CO_2 concentration decreases rapidly and the O_2 concentration increases rapidly. Finally, the period starts when the effect of boundary layer dynamics and entrainment decreases and the assimilation flux becomes the most dominant (P3), here the CO_2 concentration decreases less rapidly and the O_2 concentration increases less rapidly. We calculated a ER_{atmos} signal with equation 4, for the night-time (P1), the day-time (by either focusing on only P3 or both P2 and P3) and the complete day (P1 + P2 + P3). The exact boundaries of these periods have to be estimated. To be certain about the exact times that should be taken as the boundaries for each period, an atmospheric model is needed.

ER_{forest} is expressed as:

$$ER_{forest} = -\frac{(\overline{w'O_2'})_s}{(\overline{w'CO_2'})_s} \tag{5}$$

Where both $(\overline{w'O_2'})_s$ and $(\overline{w'CO_2'})_s$ are the mean turbulent surface fluxes above the canopy of O_2 and CO_2 over a selected time period (Seibt et al., 2004; Ishidoya et al., 2015). The *w'* in both these terms indicates the fluctuating vertical wind speed and both O_2' and CO_2' indicate the fluctuating concentrations of O_2 and CO_2. We derive the fluxes of O_2 and CO_2 using the vertical gradient (see next paragraph). The selected time periods for ER_{forest} were chosen such that the transition periods between where the respiration flux (stable atmosphere) or the assimilation flux (well mixed atmosphere) dominate, were excluded. By excluding the transition periods, we removed the periods where the gradients of both CO_2 and O_2 were close to zero. This was done because a very small gradient makes it difficult to calculate a flux and therefore the ER_{forest}, and also because during this period entrainment is the most dominant process. The exact duration of the transition periods was based on the maximum and minimum of both the friction velocity and the height of 27 m (z) divided by the Monin Obukov Length (L). The friction velocity and (z/L) indicate the measure of turbulence of the atmosphere (Stull, 1988). The mean of the remaining data points of the CO_2 and O_2 flux during the stable atmosphere period was used to calculate the ER_{forest} signal of the night and the mean of the remaining data points of the CO_2 and O_2 flux during the mixed atmosphere period was used to calculate the ER_{forest} signal of the day. The ER_{forest} for the entire day is based on the average CO_2 and O_2 flux for the entire day.

Currently, unlike for CO_2, the O_2 flux cannot be measured directly with an Eddy Covariance (EC) system. Instead, the flux can be inferred from the flux-gradient method. To calculate the flux of a certain scalar (ϕ) with the flux-gradient method, the

https://doi.org/10.5194/acp-2022-504
Preprint. Discussion started: 18 July 2022


Atmospheric Chemistry and Physics Discussions

following equation was used (Stull, 1988):

$$(\overline{w'\phi'})_s = -K_\phi \cdot \frac{\partial \overline{\phi}}{\partial z} \tag{6}$$

Where $(\overline{w'\phi'})_s$ is the surface flux, K is the exchange coefficient and $(\partial\overline{\phi}/\partial z)$ is the vertical gradient of $\overline{\phi}$. To determine the O_2 flux with Equation 6 ($\overline{\phi}$ = $\overline{O_2}$), the exchange coefficient of O_2 (K_{O_2}) needs to be determined. Ishidoya et al. (2015) assumed that K_{O_2} == K_{CO_2} and determined K_{CO_2} by dividing the CO_2 flux, measured with EC, by the CO_2 vertical gradient between two measurement levels. However, the exchange coefficient can also be determined with other methods that for example only need two measurement heights for the vertical gradient. In this study, we explore these different options for calculating K_{O_2}. The EC measurements of the CO_2 flux were used as a reference, to determine the most suitable approach. The most suitable approach to infer the O_2 flux is then used for both K_{CO_2} and K_{O_2}. During this study we derive the surface flux in the surface layer (Figure 1) and we assume that the surface flux stays constant in this surface layer, which consists of the roughness sublayer and the inertial sublayer.

We categorized the methods to determine the most suitable K into two groups: The observation-based approach (also called the K-theory (Stull, 1988) or the modified Bowen ratio method (Meyers et al., 1996)) and the theoretical approach (following the similarity theory (Dyer, 1974)). For the observation-based methods, the exchange coefficient (K) in equation 6 is determined by dividing a flux measured at 27 m, using an EC system, by a 3-height (16 m, 67 m and 125 m) vertical gradient of a specific scalar. Ishidoya et al. (2015) used this approach to calculate their O_2 flux, using the CO_2 flux and vertical gradient of two levels. Next to CO_2, we also calculated K using potential temperature (θ) for the observation-based approach. For the theoretical approach, the K in equation 6 is determined with the Monin-Obukov Similarity Theory (MOST) (Dyer, 1974), where logarithmic surface layer scaling applies for K and empirical similarity functions are used to describe the effect of atmospheric stability. In addition, we used a correction which takes into account the effect of the roughness sublayer (see Appendix for details). The SMEAR II data at 27 meter were used for the calculations with MOST. When only two heights for the gradient calculations are available, there is an option to integrate equation 6 (de Ridder, 2010). We tested both the application with and without integration in this study. We used the ICOS data, available at the SMEAR II station, for the K calculations. For the CO_2 EC measurements, we used the gap-filled data to correct for the storage below the measurement height of the EC. Gap-filling was applied when the friction velocity (u*) was below 0.4 (Kulmala et al., 2019). The Appendix gives a more elaborate explanation and provides equations of the different methods used to determine the exchange coefficients used in this study.

Finally, we select the K_ϕ that produced the best CO_2 flux results compared to the EC of CO_2, and this K was used to calculate the O_2 and CO_2 fluxes, together with the vertical gradient from measurements collected during our campaigns. For our campaigns, we only have O_2 and CO_2 measurements at two heights (23 m and 125 m), which means that $(\partial\overline{\phi}/\partial z)$ changes into $(\Delta\overline{\phi}/\Delta z)$ and the gradient was calculated with finite differences.

https://doi.org/10.5194/acp-2022-504
Preprint. Discussion started: 18 July 2022


Atmospheric Chemistry and Physics Discussions

After both the CO_2 and O_2 fluxes were determined, resulting in ER_{forest}, we subsequently calculated the $O_2 : CO_2$ exchange ratio signals for the assimilation processes (ER_a) and the respiration of the ecosystem (ER_r) with the following equations (Seibt et al., 2004; Ishidoya et al., 2015):

$$NEE = -GPP + TER \tag{7}$$

$$NEE \cdot ER_{\text{forest}} = -GPP \cdot ER_{\text{a}} + TER \cdot ER_{\text{r}} \tag{8}$$

Where the NEE is the Net Ecosystem Exchange, GPP is the Gross Primary Production and TER is the Total Ecosystem Respiration. GPP and TER are always positive by definition, representing uptake and release by the ecosystem respectively. Therefore, the resulting negative NEE values represent carbon uptake by the ecosystem, when GPP is larger than TER. We used ICOS NEE and GPP data from EC measurements from the SMEAR II station at a level of 27 meters in the 128 m height tower. First, we assumed that nighttime NEE is equal to TER, which meant that the nighttime ER_{forest} signal is equal to ER_r. We assumed that the processes that contributed to the ER_r keep the same ratio between O_2 and CO_2 during the entire day and therefore we used a constant ER_r for the entire day. Subsequently, we calculated ER_a, for both the entire diurnal cycle and the daytime using equation 8 with the corresponding ER_{forest} and the constant ER_r.

By estimating ER_r and ER_a of this boreal forest, we created the opportunity to apply atmospheric O_2 measurements to separate NEE into GPP and TER (the O_2 method). We calculated ER_r and ER_a for the representative day using equations 7 and 8, and use these to calculate GPP and TER for another representative day. We selected 13 through 15 July to create a new aggregate and to calculate a new ER_{forest} signal for the entire day. These three days were chosen because in 2019 they showed the clearest diurnal cycle of O_2 and a negative O_2 gradient, aside from 7 through 12 July, used above. By using the previously determined ER_r and ER_a, and ER_{forest} and NEE for the new representative day, we calculated GPP and TER from NEE for this new day. By comparing the GPP and TER fluxes of the O_2 method to the GPP and TER fluxes of the temperature-based function of ICOS (EC method), we could demonstrate how accurate the O_2 method is. Both Seibt et al. (2004) and Ishidoya et al. (2015) also applied the O_2 method, however both these studies used chamber measurements to first determine ER_a and ER_r and then used equation 7 and 8 to infer GPP and TER. Unfortunately we did not have chamber measurements of both O_2 and CO_2 available and therefore we used equation 7 and 8 to calculate ER_a and ER_r. This means that these two equations can be used in two ways: to determine the ER_a and ER_r signal, or to separate NEE into GPP and TER.

3 Results

3.1 O_2 and CO_2 time series

The calibrated half hourly measurements of O_2 and CO_2 for 2018 and 2019 are shown in Figure 3, together with the vertical gradients between the two measurement heights. The O_2 measurements are shown here converted from per meg to ppmEq, to allow comparison of the diurnal variability for CO_2, and to calculate the ER signals. The differences between the 23 m and

https://doi.org/10.5194/acp-2022-504
Preprint. Discussion started: 18 July 2022

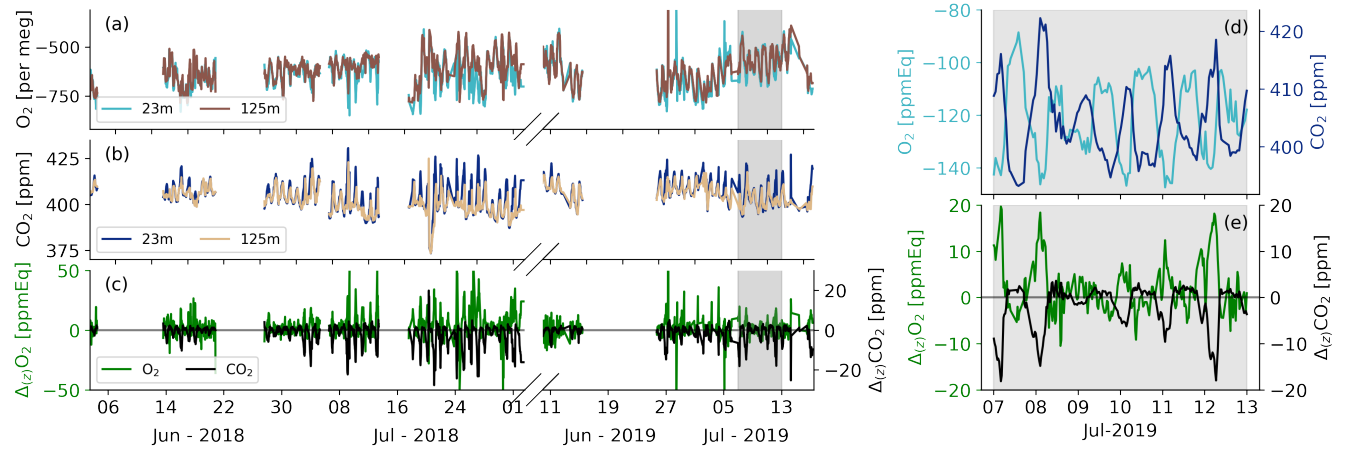

Figure 3. The half hourly average O_2 (a) and CO_2 (b) concentrations at Hyytiälä for spring/summer of 2018 and 2019 for the 125 m and 23 m height levels, together with the vertical gradient ($\Delta_{(z)}$) between these two heights (c) for both O_2 and CO_2. The shaded area indicates the dates that were selected for the aggregate representative day, 7 through 12 July 2019. The selected days are shown in more detail for the 23 m measurements (d) and the gradients (e) for both O_2 and CO_2.

125 m measurements are observable for both CO_2 and O_2. During both campaigns in 2018 and 2019, the diurnal behaviour of the O_2 concentrations has a negative relationship with the CO_2 concentrations. This negative relationship between O_2 and CO_2 is also visible from the gradient measurements, despite the relatively high uncertainty of the O_2 measurements as described in Section 2.2 and further elaborated on in Section 4.1. The period 7 through 12 July 2019 shows the most clear negative relationship between the O_2 gradient and the CO_2 gradient, and also had the most suitable meteorological conditions and was therefore selected for the aggregate representative day (Section 2.3).

3.2 Diurnal cycles

The measurements of O_2 and CO_2 and their vertical gradient for the representative day, are shown in Figure 4. There are no measurements between 20:00 and 22:00 because this is the measurement period of the calibration cylinders each day. Note that the daylight length at Hyytiälä is long at this time of the year, with sunrise at 04:00 and sunset at 23:00. We compared our CO_2 observations with ICOS CO_2 measurements at the same height, which shows that both instruments compare well overall, with a mean different of 0.70 ± 0.65 during the period 7 trough 12 July. The comparison between the two devices was a bit difficult because of the different timing of the measurements. The diurnal cycles of O_2 and CO_2 (Figure 4a) clearly show anti-correlated behaviour between CO_2 and O_2, which is especially visible during nighttime (23:00 - 04:00) and the morning transition (05:00 - 13:00).

https://doi.org/10.5194/acp-2022-504
Preprint. Discussion started: 18 July 2022

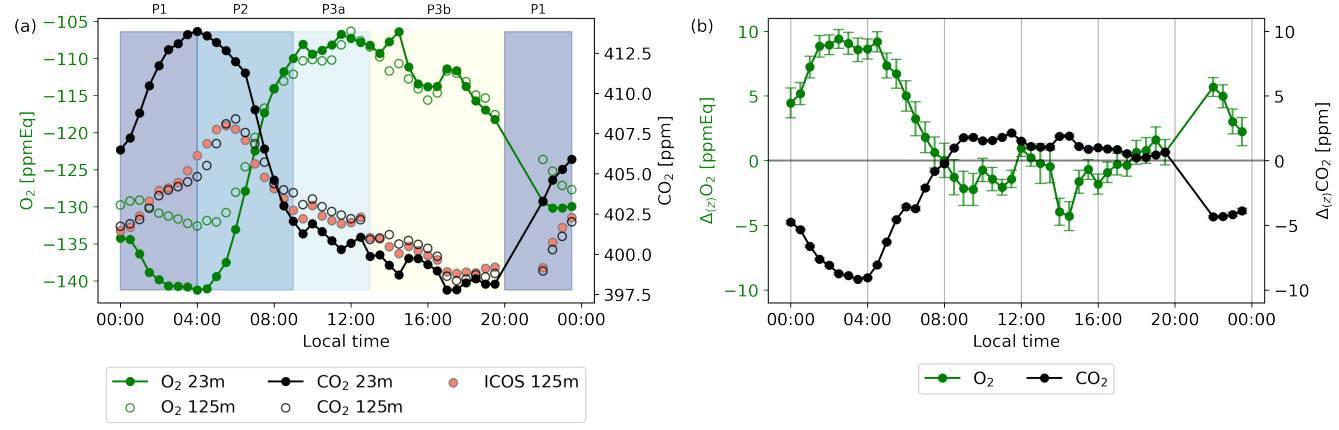

Figure 4. Diurnal cycles of the O_2 and CO_2 concentrations for the 23 m and 125 m height levels (a) and the vertical gradient between both levels with the uncertainty of both O_2 and CO_2 of the representative day, taken as the average values of 7 through 12 July 2019 (b). The CO_2 measurements of the ICOS setup are shown in (a) for comparison to the CO_2 setup measured during our campaigns. The shaded colors indicate the selected different periods where the most dominant processes are: stable atmosphere and respiration (00:00-04:00, P1), entrainment, boundary layer growth and assimilation (04:00-09:00, P2), convective conditions and assimilation (09:00-13:00, P3a), a remaining artefact after the pressure correction due to the instability of the MKS pressure regulator becomes visible during the convective conditions with assimilation dominating (13:00-20:00, P3b).

Figure 4 shows four different periods that can be linked to the periods to calculate ER_{atmos}, described in section 2.3. P1 is visible between 23:00-04:00, where respiration starts to dominate the signal and therefore the O_2 concentration decreases and the CO_2 concentration increases, in a decreasing boundary layer height dominated by thermal stratification. P2 becomes visible around 04:00 and stops around 09:00, where entrainment, the growing boundary layer and the onset of photosynthesis causes a steep increase in the O_2 concentration and a steep decrease in the CO_2 concentration. P3 can be divided into P3a and P3b and is visible between 09:00-20:00. Between 09:00-13:00 (P3a), the photosynthesis flux starts to dominate and both the O_2 and CO_2 concentration increase and decrease less rapidly. Between 13:00-20:00 (P3b) the O_2 concentration starts to decrease, while the assimilation flux still dominates, which is a remaining artefact that could not be corrected for with the pressure correction that we applied due to the instability of the MKS pressure regulator. The boundary of 20:00 between P3b and P1 was difficult to determine because we miss some measurements due to the calibration period and the remaining measurements around this time have a deviation caused by the pressure regulator. Measurements at both levels show this similar pattern, which is more pronounced closer to the vegetation.

The difference between the two heights results in a vertical gradient (Figure 4b). Similar to the diurnal cycle of the concentrations, the diurnal cycles of the gradients of O_2 and CO_2 also show anti-correlated behaviour. At 08:00, the CO_2 gradient changes from negative to positive and the O_2 gradient changes from positive to mostly negative, respectively representing CO_2 being transported downwards and O_2 upwards. The magnitude of the gradient depends on the degree of vertical mixing. The

https://doi.org/10.5194/acp-2022-504
Preprint. Discussion started: 18 July 2022

Atmospheric Chemistry and Physics Discussions

sign of the gradients changes during the day, because the lowest level (23 m) is more directly influenced by forest carbon exchange compared to the highest level (125 m). Around the time of sunset, the CO_2 gradient changes from positive to negative and the O_2 gradient changes from negative to positive, because the lowest measurement level (23 m) is now influenced more by respiration processes of the forest and soils compared to the highest measurement level (125 m).

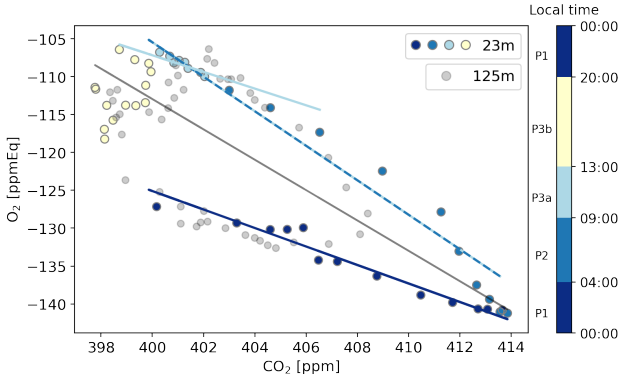

Figure 5. The O_2 concentration plotted against the CO_2 concentration for the representative day, for the 23 m level in coloured points per period representing different dominant process and the 125 m level in grey points. The dominant processes are: respiration (00:00-04:00), entrainment (04:00-09:00), assimilation (09:00-13:00), a remaining artefact after the pressure correction due to the instability of the MKS pressure regulator becomes visible (13:00-20:00). The regression lines indicate the exchange ratio of the atmosphere (ER_{atmos}) during the time with a specific dominant process.

By using equation 4, we calculated four distinctly ER_{atmos} signals for different periods throughout the day at 23 m, and to a smaller degree at 125 m (Figure 5 and Table 3). The same periods as shown in Figure 4 are visible in Figure 5. This results in an ER_{atmos} during the night (P1) of 1.22 ± 0.02 and two different possibilities for the ER_{atmos} signal during daytime. By combining both P2 and P3a we get a signal of 2.28 ± 0.01 and by focusing only on P3a, which excludes the entrainment and the boundary layer dynamics, we get a signal of 1.10 ± 0.12. Last, by combining all the periods (P1, P2, P3) we get a signal for the complete day of 2.05 ± 0.03. The uncertainties given here only represent the uncertainty of the slopes from the regression lines in Figure 5. The high values for the ER_{atmos} signal of the entire day and the daytime signal that includes entrainment and the boundary layer dynamics are not very realistic to represent an ER for the forest, and shows that we should be careful when using ER_{atmos}. This will be elaborated on in Section 4.2.

3.3 Flux calculations for CO_2 and O_2

We explored four alternative methods to derive the O_2 flux from the vertical gradient of the two measurement levels, as described in Section 2.3. Figure 6 shows both the theoretical and the observation-based approach that were used to calculate the

https://doi.org/10.5194/acp-2022-504
Preprint. Discussion started: 18 July 2022

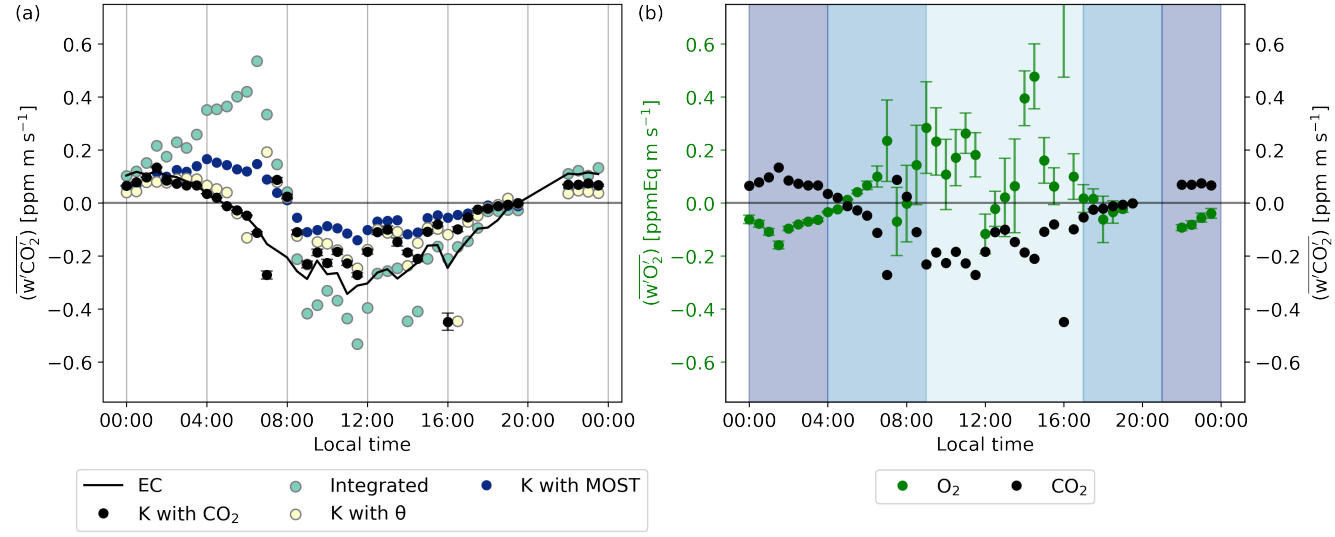

Figure 6. The CO_2 flux (a) calculated with different methods for the representative day, as described in Section 2.3, compared to the CO_2 flux of the ICOS EC measurements. (b) the comparison between the O_2 and CO_2 flux calculated using the method that gave the best results for the CO_2 flux calculations (using the exchange coefficient K with CO_2), for the representative day. The shaded colours indicate the regions that were selected for: the night signal (21:00-04:00), the day signal (09:00-17:00) and the remaining regions (04:00-09:00 and 17:00-21:00)

CO_2 flux and the comparison with the ICOS EC CO_2 flux measurements at 27 m on the tower. By comparing these approaches to the EC measurements, we determined which method is most suitable to calculate the O_2 flux. The CO_2 flux measured by the EC system stays positive until around 05:00, when the respiration fluxes are the most dominant and the nocturnal boundary layer is shallower. After 05:00, the CO_2 flux of the EC system becomes negative, and the forest begins to take up CO_2 instead of emitting it. The assimilation fluxes increase and exceed the respiration fluxes, the boundary layer starts to grow and air with lower CO_2 concentrations is entrained from the free troposphere. After 20:00, the CO_2 flux of the EC system becomes positive again because the assimilation fluxes decrease, and the respiration signal begins to dominate again while the boundary layer height decreases. We expect to find this diurnal pattern and the sign change in our calculations of the CO_2 flux from the vertical gradient method as well.

First, we discuss the theoretical methods, that are indicated in Figure 6 with 'K with MOST' and 'Integrated' approach (see Section 2.3). The MOST and the Integrated method both overestimate the CO_2 flux during the night, between 0:00 and 05:00. The resulting CO_2 flux furthermore decreases and becomes negative too late in the day compared to the EC measurements. Both the CO_2 flux of the MOST and Integrated method evolve from a positive flux to a negative flux around 8:00. This is three hours later than the CO_2 flux from the EC measurements. During the day, between 08:00 and 15:00, the K with MOST method underestimates the CO_2 uptake and the Integrated method overestimates it. Table 2 shows that both MOST and the Integrated method have the highest mean difference and Root Mean Square Error (RMSE) compared to the observation-based

https://doi.org/10.5194/acp-2022-504
Preprint. Discussion started: 18 July 2022


Atmospheric Chemistry and Physics Discussions

approaches. We discuss this further in section 4.3. As result of this analysis, we decided to not use the theoretical approach to calculate the O_2 flux.

Table 2. The mean difference and the Root Mean Square Error (RMSE) of the comparison between the CO_2 flux of the EC CO_2 flux measurements at 27 m in the tower and the CO_2 flux calculated with different methods for the exchange coefficient K, based on the ICOS data, and using the vertical gradient of CO_2 at 23 m and 125 m of our campaign data.

Approach for K	Mean difference [ppm m s^{-1}]	RMSE [ppm m s^{-1}]
Integrated	0.123	0.184
K with MOST	0.117	0.138
K with θ	0.087	0.114
K with CO_2	0.066	0.092

Secondly, we analyze the observation-based approaches, that are indicated in Figure 6 with 'K with θ' (where K is established using potential temperature) and 'K with CO_2' (where K is established using CO_2). The observation-based approaches showed a better comparison with the EC observations in determining the CO_2 flux compared the to theoretical approach. Both the θ and the CO_2 method represent satisfactorily the nocturnal CO_2 flux between 0:00 and 5:00. After 5:00, the fluxes calculated by both methods start to decrease and change sign around the correct time (5:00) from a positive to a negative flux. During the day between 8:00 and 15:00, both the θ and the CO_2 methods underestimate the CO_2 flux, but not as much as the theoretical methods. Table 2 also shows that both the θ and the CO_2 methods have the lowest Mean difference and RMSE. Based on the smaller mean difference and RMSE, and the direct link of CO_2 with O_2, we decided to proceed with the method where K is calculated with the ICOS data of CO_2 to calculate the O_2 flux, instead of the ICOS θ data. This K was then multiplied with our measured O_2 vertical gradient between 23 m and 125 m to finally calculate the O_2 flux. Section 4.3 presents a more elaborate discussion on the different methods to determine the most suitable K.

The resulting O_2 flux calculated with the exchange coefficient K based on the ICOS CO_2 data is shown in Figure 6b. The uncertainties are based on the error propagation of the standard error of the 30-minute averaged CO_2 and O_2 measurements. The daytime flux values have a high variability, but the inferred fluxes appear physically realistic and promising for one of the first attempts to calculate O_2 fluxes. During the night, between 0:00 and 5:00, the O_2 flux data has a relatively stable negative value. The O_2 flux is negative during the night, because the forest consumes O_2 for the respiration processes while CO_2 is released and this leads to a positive CO_2 flux during the night. After 5:00, the O_2 flux becomes positive and shows a higher variability. Overall, the O_2 flux is positive during the day which indicates that the forest produces O_2 because of the higher assimilation rate compared to the respiration. The high variability of the O_2 flux compared to the CO_2 flux, is caused by the less precise measurements of the O_2 vertical gradient compared to the CO_2 gradient (Figure 4). The measurement precision

https://doi.org/10.5194/acp-2022-504
Preprint. Discussion started: 18 July 2022

Atmospheric Chemistry and Physics Discussions

needed to measure the difference between the two levels is very high, and therefore impacts the measurement of the gradient of O_2. The nighttime values of the O_2 flux are therefore more reliable compared to the daytime values, since the difference between the two heights is larger and therefore easier to measure due to the more stable atmospheric conditions at night .

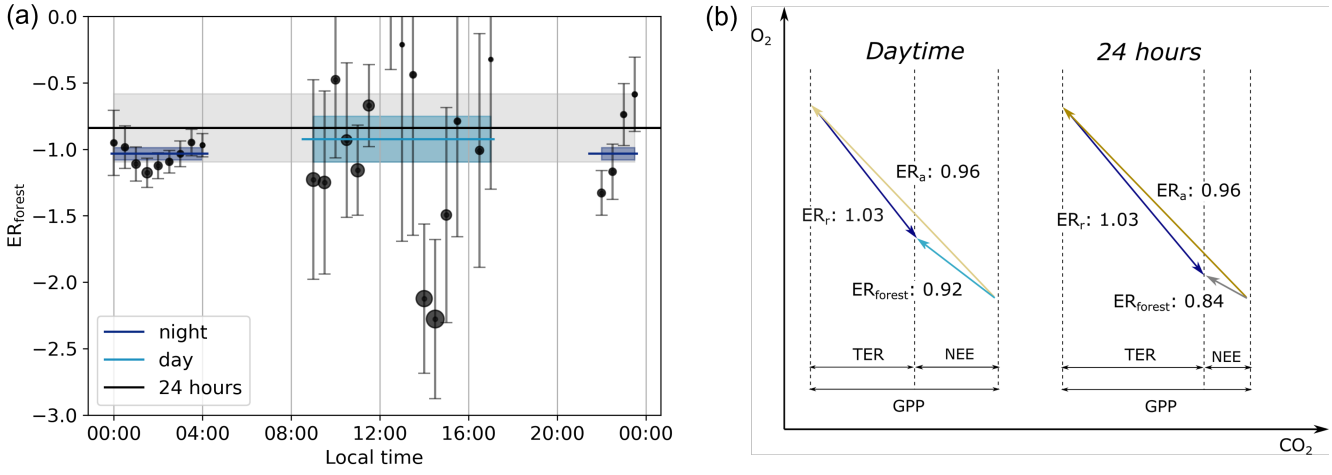

Figure 7. The half-hourly exchange ratio of the forest (ER_{forest}) and the resulting averaged ER_{forest} for the entire day (black line), the night between 21:00-4:00 (dark blue line) and the day between 9:00-17:00 (light blue line), of the representative day (a). The size of the dots indicates the size of the absolute O_2 flux and the shaded bands indicate the uncertainties of the different ER_{forest} signals. Note that the ER_{forest} lines do not match with the average of the dots in the specific time period, because the lines are based on the averaged fluxes. These different ER signals are presented in a vector diagram format with the carbon fluxes, Gross Primary Production (GPP), Total Ecosystem Respiration (TER) and Net Ecosystem Exchange (NEE), and the ER of the assimilation processes (ER_a) and the ER of the respiration processes (ER_a) (b).

By using equation 5, we find three different ER_{forest} signals throughout the day (Figure 7 and Table 3). The selected time periods based on the criteria described in Section 2.3 are between 09:00-17:00 for the daytime and between 21:00-04:00 for the nighttime (Figure 6). This results in a nighttime ER_{forest} signal of 1.04 ± 0.04, a daytime ER_{forest} signal of 0.92 ± 0.17 and an ER_{forest} signal for the entire 24 hours of 0.83 ± 0.24. Note that this 24h value is not the average of the day and night ER_{forest} signals or from all the 30-minute ER_{forest} signals, because we used the averaged fluxes. This means that the ER_{forest} signals based on high flux values, indicated in Figure 7 with larger symbols, contribute more to the averaged ER_{forest} signals compared to the lower flux values. The individual ER_{forest} values of every 30-minutes show a clear difference between the day- and nighttime. The ER_{forest} values during the nighttime is relatively stable. The ER_{forest} values during the daytime show more variability, caused by the high variability of the O_2 flux during daytime (Figure 6). The uncertainty of the ER_{forest} signals is determined by the propagation of the standard error of the 30-minute average O_2 and CO_2 measurements.

https://doi.org/10.5194/acp-2022-504
Preprint. Discussion started: 18 July 2022

Atmospheric Chemistry and Physics Discussions

3.4 GPP and TER calculations

Table 3. The exchange ratio for the atmosphere (ER_{atmos}: Section 3.2), the forest (ER_{forest}: Section 3.3), and assimilation and respiration (ER_a and ER_r: section 3.3) for different time periods of the representative day. The time periods used to calculate the signals are: (09:00-13:00) for day and (23:00-04:00) for night of ER_{atmos}, and (09:00-17:00) for day and (21:00-04:00) for night of ER_{forest}, ER_r and ER_a. Note that the uncertainty for ER_{atmos} does not represent the same uncertainty as for ER_{forest}, since the first is the error of the fit, and the second is based on error propagation of the half hourly measurements.

	ER_{forest}	ER_r	ER_a	ER_{atmos}
Night	1.03 ± 0.05	1.03 ± 0.05		1.22 ± 0.02
Day	0.92 ± 0.17	1.03 ± 0.05	0.96 ± 0.12	1.10 ± 0.12
24 hours	0.84 ± 0.26	1.03 ± 0.05	0.96 ± 0.11	2.05 ± 0.03

We found the ER signals for assimilation (ER_a) and respiration (ER_r) by using equation 8 (Figure 7b and Table 3). The assumption that ER_r stays constant throughout the day seems reasonable, because the ER_{forest} values stay stable during the night. Therefore the ER_r signal becomes 1.03 ± 0.05. ER_a of the daytime is 0.96 ± 0.11, which indicates the ER_a signal of the boreal forest when the surface fluxes are the highest. The ER_a signal of the entire diurnal cycle is 0.95 ± 0.11, which also includes the assimilation processes during sunrise and sunset. Figure 7b shows all these ER signal and how they change throughout the day, together with their carbon fluxes. ER_a, ER_r and the resulting ER_{forest} signals are more realistic compared to the ER_{atmos} signals and these differences will be further elaborated on in Sections 4.4 and 4.5.

By using equation 7 and 8 and ER_a and ER_r signals determined from the representative day, we show that the O_2 method can be used to separate NEE into GPP and TER on any day where good simultaneous CO_2, O_2 and NEE measurements are available (Figure 8). The difference between the CO_2 fluxes determined with the O_2 method and the EC method of both the GPP and the TER flux are around 0.01 ppm m s^{-1}, which is less that 6% of the total gross flux. The difference is relatively small which means that the O_2 method compares well with the EC methods to separate NEE into GPP and TER. The different uncertainty bars in Figure 8) show how sensitive the O_2 method is to the accuracy of ER_{forest}. By increasing/decreasing ER_{forest} with 0.2, the GPP estimation by the O_2 method changes by 0.1 ppm m s^{-1} and by increasing/decreasing ER_{forest} with only 0.01, the GPP estimation changes with 0.005 ppm m s^{-1}. The effect of changing ER_{forest} on TER has the same effect on GPP. This shows that the O_2 method is quite sensitive to ER_{forest} and should be measured accurately, with a suggested precision of around 0.05. The application of the O_2 method will be further discussed in Section 4.5.

4 Discussion

We aimed to advance understanding of the O_2 : CO_2 exchange ratio and its diurnal variability over a boreal forest by continuously measuring both O_2 and CO_2 concentrations at two heights above the canopy. These measurements gave us the possibility

https://doi.org/10.5194/acp-2022-504
Preprint. Discussion started: 18 July 2022

Atmospheric Chemistry and Physics Discussions

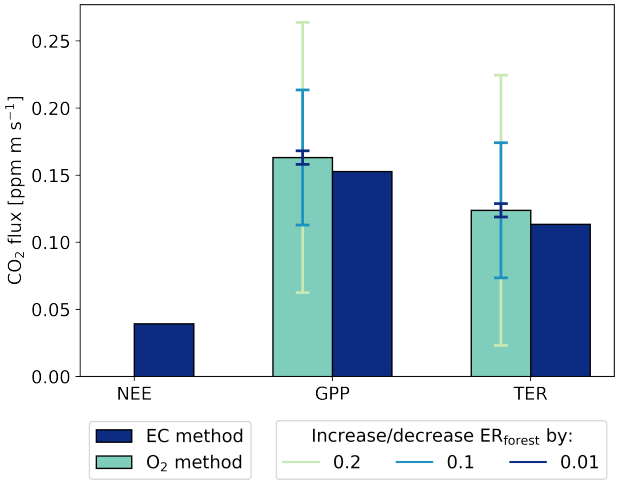

Figure 8. The CO_2 fluxes of a second representative day (13 through 15 July) for Net Ecosystem Exchange (NEE), Gross Primary Production (GPP) and Total Ecosystem Exchange (TER) based on two different methods: the EC method and the O_2 method. The different uncertainty bars indicate an increase/decrease of 0.2, 0.1 or 0.01 for the Exchange Ratio of the forest (ER_{forest}), used in the O_2 method.

to compare the ER_{atmos} and ER_{forest} signal of an aggregate representative day and compare the boreal forest signals to previous studies in different ecosystems. Our ER_{atmos} signal changed between the day (2.28) and the night (1.22) and had an overall diurnal signal of 2.05. For the ER_{forest} signal, we needed to determine the O_2 and CO_2 surface fluxes based on the two heights. Different flux calculating methods were compared. The O_2 flux was calculated with the method that resulted in the best comparison to Eddy Covariance fluxes for CO_2, where we found that the exchange coefficient K based on the CO_2 data was most suited. The resulting ER_{forest} signal showed again differences between the day (0.92) and night (1.04) and the overall diurnal ER_{forest} was 0.83. For these differences and variability in the ER signals, different aspects of the uncertainty have to be taken into account, on which we elaborate in the next sections.

4.1 Measurement uncertainty

Analyzing the mean difference and standard deviation of the target cylinder values between 16-06-2019 and 17-07-2019 (Table 1), we see that the values are relatively high. Previous studies that used a fuel cell analyser for continuous atmospheric O_2 measurements (Battle et al., 2019; Ishidoya et al., 2013; van der Laan-Luijkx et al., 2010; Popa et al., 2010; Pickers et al., 2022), achieved measurement precision of around 5 per meg. WMO recommends a maximum compatibility of 10 per meg for the world-wide O_2 monitoring network (Crotwell et al., 2020), which shows that our measurement precision of 19 per meg is relatively poor. This poor measurement precision could have been caused by several reasons; the O_2 values of the reference cylinders that were used were relatively far apart, making it more difficult to measure the values around the target cylinder value. The cabin in which the instrument and cylinders were located was not well insulated, which created unstable temperature conditions which might have affected the stability of the cylinders (Keeling et al., 2007). Our calibrations took place

https://doi.org/10.5194/acp-2022-504
Preprint. Discussion started: 18 July 2022


Atmospheric Chemistry and Physics Discussions

during the night and therefore large temperature changes during the day might have affected daytime stability of the reference cylinder. Furthermore, tiny leakages in the setup might have influenced the measurements. Due to the relatively short period for these campaigns and remote location, it is not possible to trace back the cause of this large uncertainty. This high uncertainty resulted in a larger uncertainty of the vertical gradient of the two heights of the O_2 measurements. However, in this study we are mostly interested in the diurnal variability of the ER signal and differences between ER_{atmos} and ER_{forest} and therefore the long-term stability of the measurements are less relevant here compared to other O_2 studies.

To reduce the effect of the high measurement uncertainty and derive a more statistically robust signal of the vertical gradient, we created an aggregate representative day based on days with similar weather and atmospheric conditions. This representative aggregate day removes the focus from one specific day, and therefore decreases the effect of the low measurement precision. We also move away from the reality of one specific day, but rather focus on an average situation and variability of the ER signal above a boreal forest based on O_2 and CO_2 measurements at 2 levels. Given that only very few previous studies focused on deriving forest ER signals globally, our analysis helps to gain further understanding of the diurnal variability and the difference between ER_{atmos} and ER_{forest}, which will be discussed in the following sections.

4.2 ER_{atmos} signal in comparison to previous studies

Despite the uncertainty in our measurements, there are clear differences between the slopes of O_2 and CO_2 throughout the diurnal cycle (Figure 5). Three different ER_{atmos} signals are visible, with two signals for the day (2.28 ± 0.01 and 1.10 ± 0.12) and one for the night night (1.22 ± 0.02) slope (Table 3). Note that the uncertainty of these values is based on the slope of the fitted line in Figure 5 and does not represent the uncertainty in the stability of our measurements as indicated in Table 1. The difference between day and night values of ER_{atmos} was expected because different processes (i.e. respiration, assimilation and entrainment) with different ER signals play a role at different times during the diurnal cycle. To exclude as much as possible the effect of entrainment and the boundary layer dynamics during the morning transition, we will from now on refer to the 1.10 value as the day ER_{atmos} signal, which is the signal derived form period P3a. ER_{atmos} for the complete day results in 2.05 ± 0.03.

When comparing our ER_{atmos} signals to those from Battle et al. (2019), Ishidoya et al. (2013) and Seibt et al. (2004) (Table 4), we note several similarities but also some differences regarding the specific values of the ER_{atmos} signals. Our daytime signal of 1.10 is similar to 1.02, 0.87 and 1.14 from the previous studies respectively, as is our nighttime signal of 1.22 compared to 1.12 (Battle et al., 2019), 1.03 (Ishidoya et al., 2013) and 1.16 (Seibt et al., 2004). However, our 24-hours ER_{atmos} signal of 2.05 shows an unrealistically high number which clearly does not indicate the ER of the forest only. A typical ER_{atmos}signal for a 24 hour period lies around 1, as is shown in table 4 and by Stephens et al. (2007) and Manning (2001). Our 24-hours ER_{atmos} value includes the measurement points of the period that is influence by entrainment and boundary layer dynamics (P2), for which period we found an ER signal of 2.28. The large influence of entrainment and boundary layer dynamics made it difficult to be very precise about the specific time periods to choose for P3. Moving the selected time boundaries of P3a from 9:00 to 9:30 or from 13:00 to 12:30 leads to ER_{atmos} values of 0.88 or 1.75 respectively. The large changes in the daytime ER_{atmos}due to

https://doi.org/10.5194/acp-2022-504
Preprint. Discussion started: 18 July 2022

Atmospheric Chemistry and Physics Discussions

Table 4. The different Exchange Ratio (ER) signals of previous studies, with the ER of the atmosphere (ER_{atmos}), the ER of the forest (ER_{forest}), the ER of the respiration processes (ER_r) and the ER of the assimilation processes (ER_a). The different studies are: Bat, 2019: (Battle et al., 2019), Ish, 2015: (Ishidoya et al., 2015), Ish, 2013: (Ishidoya et al., 2013), Sei, 2004: (Seibt et al., 2004).

	$\mathbf{ER_{atmos}}$ [a]			$\mathbf{ER_{forest}}$ [b]				
Study	Day	Night	24 hours	Day	Night	24 hours	ER_r	ER_a
This study	1.10 ± 0.12	1.22 ± 0.02	2.05 ± 0.03	0.92 ± 0.17	1.03 ± 0.05	0.84 ± 0.26	1.03 ± 0.05	0.96 ± 0.12
Bat, 2019	1.02 ± 0.01	1.12 ± 0.01						
Ish, 2015				< 1.0	> 1.0	0.86 ± 0.04	1.11 ± 0.01	1.0
Ish, 2013	0.87 ± 0.02	1.03 ± 0.02	0.94 ± 0.01	≈ 0.98	≈ 1.11	0.89	1.11 ± 0.01	1.02 ± 0.03
Sei, 2004[c]			1.01 ± 0.06	1.24 ± 0.06	1.01 ± 0.02	1.26 ± 0.05	0.94 ± 0.04	1.19 ± 0.12
Sei, 2004[d]	1.14 ± 0.19	1.16 ± 0.02	1.03 ± 0.05					

[a] An ER signal is classified as ER_{atmos} when the ER signal is based on one concentration measurement of O_2 and CO_2.

[b] An ER signal is classified as ER_{forest} when the ER signal is based on surface fluxes from either an 1-box model or vertical gradient flux calculations.

[c] The ER signals of the location Griffin Forest of Seibt et al. (2004) are used here.

[d] The ER signals of the location Harvard Forest of Seibt et al. (2004) are used here.

small changes in the time boundaries, shows the high uncertainty of the daytime ER_{atmos}. Therefore, our measurements provide a confirmation of earlier indications (Seibt et al., 2004) that ER_{atmos} is an unreliable estimate for the ER of a forest, and we recommend to use ER_{forest}. Instead, ER_{atmos} also represents how O_2 and CO_2 are influenced by the boundary layer dynamics and entrainment (Figure 1).

For the 24-hour period, our ER_{atmos} values are much higher compared to previous studies. A possible explanation could be that our study is the first to measure O_2 and CO_2 above a boreal forest. Boreal forests have different ecosystems, a colder climate and have longer days in the summer compared to the locations of the previous studies (Bonan, 2008). The measurements of Battle et al. (2019) and Ishidoya et al. (2013) were done over a deciduous forest and measurements of Seibt et al. (2004) over a needle leaf forest and mixed deciduous forest, all conducted in temperate regions. A change in the length of the day or temperature could already influence the diurnal cycles of both the O_2 and CO_2 concentrations and as a result ER_{atmos} (Figure 1). A high ER_{atmos} signal means the O_2 concentration increases more rapidly over time compared to the decrease of the CO_2 concentration. Further insights on the contributions of each process to ER_{atmos} cannot be estimated from the measurements alone, and would require using an atmospheric model.

4.3 Uncertainties in the CO_2 and O_2 flux calculations

By comparing the theoretical and observation-based methods, we determined that the most suitable method to calculate both the CO_2 and O_2 flux was to use the observation-based method with CO_2 data (Section 3.3). Figure 6 and Table 2 show that the

https://doi.org/10.5194/acp-2022-504
Preprint. Discussion started: 18 July 2022


Atmospheric Chemistry and Physics Discussions

theoretical methods (MOST and Integrated) resulted in a too late change of the CO_2 flux compared to the EC-measurement. This delay has been described before and is caused by the time it takes before the turbulence can mix the CO_2 gradient driven by stable nocturnal stratification conditions and establish the corresponding gradient (Casso-Torralba et al., 2008). When the heights of the gradient are closer together, the delay is less pronounced. However, the measurement heights used during our campaign are relatively far apart (125 m and 23 m) and the EC flux is measured at 27 m. The 125 m measurement is even located outside the surface layer during the morning transition. This made the flux-gradient method less applicable, which assumes that the surface flux stays constant in the surface layer (Dyer, 1974).

Since during our campaign we only measured at two heights, we missed information on the logarithmic profile originating from the canopy top, which resulted in an underestimation of the flux using the K with MOST. This was solved by integrating the MOST equation ('Integrated method'). With the integrated method, the gradient is assumed to be logarithmic and the total flux increases compared to the MOST calculation (Paulson, 1970). However, with the large difference between the two measurement heights, the integrated approach still overestimated the CO_2 flux compared to the EC measurements during both the day and the night. Also, the delay in the timing of the sign change of the gradient cannot be solved with this Integrated method. We furthermore applied the effect of the Roughness Surface Layer (RSL) in the flux calculations of the theoretical methods, by adding an extra factor that accounts for this layer (not shown in the results) (de Ridder, 2010). The contribution of the RSL did not improve our results, because it also includes the delay of the gradient which was causing the largest deviation in the theoretical methods (Table 2).

By applying both observation-based methods, using either θ or CO_2 to infer the exchange coefficient K, we did not find this delay in the timing of the gradient and the observation-based methods therefore resulted in derived fluxes close to the EC measurements. Here it has to be noted that the ICOS EC measurements of CO_2, that we used as a benchmark for the most suitable flux calculation approach, was also used in calculating K with CO_2, which makes the comparison of these approaches to the CO_2 flux not fully independent. Most previous studies that determined fluxes based on the gradient-approach used θ to calculate K (Stull, 1988; Mayer et al., 2011; Wolf et al., 2008; Bolinius et al., 2016; Brown et al., 2020), because θ is the driver of convective turbulence. However, because O_2 is directly linked to CO_2 and our statistics (Table 2) indicated that the CO_2 method resulted in a better comparison to the EC fluxes, we decide to use the ICOS CO_2 data at 3 levels and the CO_2 EC measurements to calculate K. This K together with the measurements of two heights by our instrument during our campaign were used to calculate both the CO_2 and the O_2 fluxes used in our study. We also tested the impact of using only 2 vertical levels of the ICOS CO_2 concentrations to calculate K (not shown), which was also the case in the only previous study that derived O_2 fluxes. Ishidoya et al. (2015) derived O_2 fluxes for a temperate forest in Japan using 2 vertical levels at 18 and 27 m height for both O_2 and CO_2 concentrations. Our comparison of deriving K based on 2 vertical levels (23 m and 125 m), resulted in an underestimation of the gradient and thus an overestimation of K, and as a consequence the calculated CO_2 flux was overestimated. Therefore the 3 levels of ICOS CO_2 concentrations measurements proved to be vital in our flux calculations here. We still missed the logarithmic profile at the surface with only the two vertical campaign measurements and as a result

https://doi.org/10.5194/acp-2022-504
Preprint. Discussion started: 18 July 2022


Atmospheric Chemistry and Physics Discussions

slightly underestimated the final CO_2 and O_2 flux. Therefore, we recommend to always measure at at least three heights of CO_2 and O_2 inside the surface layer, when they are meant to be used for flux calculations.

Our final O_2 flux (Figure 6) shows a clear diurnal cycle, with the expected behaviour of negative values in the night (O_2 consumption for respiration) and a positive flux during the day (O_2 release during assimilation). The nighttime fluxes are more stable and give a clear signal due to the larger vertical gradient. K is more difficult to determine during the night because the EC measurements are less representative due to the low level of turbulence. However, the largest contributor to the uncertainty are our own O_2 measurements and the larger gradient allows to better establish the O_2 flux. The larger variability of the daytime O_2 fluxes is caused by the smaller gradient of the O_2 concentration measurements during the day (Figure 3), when the atmosphere is more well-mixed and the difference between the two heights becomes smaller. The relatively large measurement uncertainty made it difficult to measure these small difference between the two heights and increased the noise in the fluxes. The measurement noise resulted in O_2 gradient variations that were not tied to the CO_2 gradient variations and this degraded the correlation between the two fluxes. Despite this larger variability, we still find a clear diurnal behaviour, which allowed us to calculate ER_{forest}.

4.4 ER_{forest} signal compared to previous studies

Our resulting ER_{forest} signal changes throughout the diurnal cycle, with specific daytime (0.92 ± 0.17), nighttime (1.03 ± 0.05) and overall (0.84 ± 0.26) values (Figure 7 and Table 3). The individual nighttime values show a smaller uncertainty due to the already explained effect of the larger gradient during the stable atmospheric conditions of the night. In contrast, the individual daytime values show a larger uncertainty due to the smaller gradient during the unstable atmospheric conditions of the day. We therefore used averaged values for the daytime and nighttime signals to derive the ER_{forest} values. The daytime signal excludes the entrainment and the boundary layer dynamics during the morning transition, however these effects are still included in the overall ER_{forest} signal.

When comparing our ER_{forest} signals to previous studies of Seibt et al. (2004), Ishidoya et al. (2013, 2015) (Table 4) we notice that the difference between the daytime and the nighttime values that we found and the specific values of the different ER_{forest}, have some similarities and some differences. Our results, together with Ishidoya et al. (2013, 2015) (night: 1.11 and day: 0.98) show that the ER_{forest} signal of the nighttime is higher than the the daytime signal, whereas Seibt et al. (2004) (day: 1.24 and night: 1.01) showed the opposite behaviour. Our results is most similar to the signals of both Ishidoya et al. (2013) and Ishidoya et al. (2015), especially if we take our uncertainty range into account. When we take into account our uncertainty, the complete day signal of 0.84 ± 0.26 comes close to the globally used average ER of the biosphere of 1.1 (Severinghaus, 1995). However, the specific value suggest that the overall ER_{forest} signal of this boreal forest lies somewhat lower than 1.1, closer to 1.0. Why the ER_{forest} signals differ between studies could be explained with the different ER_a and ER_r signals, which

https://doi.org/10.5194/acp-2022-504
Preprint. Discussion started: 18 July 2022


Atmospheric Chemistry and Physics Discussions

will be discussed in section 4.5.

The ER_{forest} and ER_{atmos} signals are not identical, and they do therefore not represent the same information (Table 3). The ER_{atmos} signals are higher compared to the ER_{forest} signals, especially the 24-hour signals show a large difference. Despite the higher numbers, the day and night signals of ER_{atmos} and ER_{forest} show both the same pattern, where the daytime signal is lower compared to the nighttime signal. When comparing these differences to previous studies we find that not all studies find the same results. The difference between ER_{forest} and ER_{atmos} was not found by Ishidoya et al. (2013). In contrast, Seibt et al. (2004) found a difference between ER_{forest} and ER_{atmos} (Table 4). These contradicting results suggest that we should further investigate to what extent ER_{atmos} is influenced by entrainment and boundary layer dynamics and under which conditions they can come close to ER_{forest}. We already show that excluding the morning transition (P2) helps to improve the ER_{atmos} signal. However, as already stated, it is difficult from the measurements alone to determine if the ER_{atmos} signal is influenced only by the surface during this period. An Atmospheric model would therefore be needed to find how ER_{atmos} can be derived from a single measurement height, and allow comparison to previous studies that measured at one height to determine the ER of the forest (Battle et al., 2019; van der Laan et al., 2014; Stephens et al., 2007). We are currently applying a specific mixed-layer atmospheric model to further investigate this.

4.5 The ER_a and ER_r signals

To further understand the relationship between O_2 and CO_2, we cannot use the ER_{forest} signal alone. To look in more detail into the processes driving the variations, we look at the exchange ratio of respiration (ER_r) and assimilation (ER_a). Due to lack of in-situ measurements of ER_a and ER_r, we calculated these numbers (Table 3 and Figure 7). ER_r was taken as the ER_{forest} night-time signal (1.03 ± 0.05), by assuming that only respiration influences the ER_{forest} signal during the night and that the ER_r signal stays constant throughout the entire day. This means that both the heterotrophic and autotrophic respiration are included in ER_r and the same components are respired in the same ratios throughout the day to keep ER_r a constant value. To our knowledge, potential changes of ER_r throughout the day have not been studied previously, and it is therefore difficult to say how valid this assumption is. The variability of ER_r between locations highly depends on the soil properties (Angert et al., 2015), which makes it difficult to compare with the few studies available (Seibt et al., 2004; Ishidoya et al., 2013) that measured ER_r with chamber measurements on a brown soil. The soil in our study area is a podzol, which is characterised by a high acidity with little organic matter (Buurman and Jongmans, 2005). The OR of podzols is around 1.08 (Worrall et al., 2013) and the ER of acid soils is expected to be around this OR, because carbon cannot easily dissolve into the groundwater (Angert et al., 2015), and we therefore conclude that our ER_r value of 1.04 is realistic.

We looked at two options to calculate ER_a; ER_a based only on the daytime measurements (between 9:00 and 17:00: 0.96 ± 0.12) and ER_a based on all the measurement throughout the 24-hour period: 0.96 ± 0.11). Both numbers are close to 1, which is often assumed as a standard value for ER_a (Ishidoya et al., 2015; Severinghaus, 1995). Next to that, a value of ER_a close to

https://doi.org/10.5194/acp-2022-504
Preprint. Discussion started: 18 July 2022


Atmospheric Chemistry and Physics Discussions

1 means that ammonium is used as a source for nitrogen, instead of nitrate (Bloom et al., 1989, 2012). Ammonium is indeed a larger source for nitrogen compared to nitrate in Hyytiälä (Korhonen et al., 2013). The OR of needle leaves, and plant material in general, appears to be always close to 1.0 (Jürgensen et al., 2021), which again confirms our ER_a signals. The difference between the two ER_a signals is minimal and difficult to determine with the corresponding uncertainties. The transition periods between the night and the daytime were difficult to measure, because the gradient then becomes close to zero, which means there could be a possibility that next to ER_{forest}, ER_a also has a diurnal cycle. To get a more detailed overview of ER_a, more precise measurements need to be done with an uncertainty that is lower than 0.1 for the ER signals. However, the simular values of ER_a for the daytime and all the measurements means that ER_a does not have a major shift because of entrainment during the morning transition and it would suggest that the morning transition is less of an issue for ER_{forest} than for ER_{atmos}.

By applying the O_2 method to a new aggregate day, we showed that the O_2 method gives results similar to the EC method to derive the GPP and TER fluxes (Figure 8). The EC method to separate GPP and TER fluxes, also contains uncertainties in the approach, because of the assumption to rely on a function of temperature, and should therefore not necessarily be assumed to be the 'truth' (Reichstein et al., 2005). Despite the uncertainty of both the O_2 method and the EC method, both methods give similar results for the CO_2 flux of GPP and TER. For the O_2 method, the magnitude of the GPP and the TER fluxes highly depends on the ER_{forest} signal used and that this signal should be measured with an accuracy of around 0.05 to fall into the uncertainty range of the EC method. With such a high accuracy, the O_2 method has the potential to provide an alternative method for the separation of GPP and TER without relying on the regularly used temperature-based function (EC method). Ishidoya et al. (2015) showed similar results, where the O_2 method also produced GPP and TER comparable to the EC method and the magnitude of the GPP and TER fluxes highly depended on the ER_a and ER_r signals. We recommend to measure the ER_r and ER_a signals directly with chamber measurements (Seibt et al., 2004; Ishidoya et al., 2013), together with adding at least one measurement height for the O_2 and CO_2 concentrations below the canopy. This can help to get a better understanding of how the different signals travel from the surface towards the atmosphere and how to apply the storage correction for both the O_2 and the CO_2 fluxes (Aubinet et al., 2012). Despite the high dependency on the accuracy of the ER, this study showed again, as did (Ishidoya et al., 2015), that the O_2 method can be used to get a better understanding of the carbon cycle. To further develop this method we need to expand the O_2 measurements for longer time series and more locations, and analyze how ER_{forest} varies over longer time scales, which can improve the global average value of ER (α_B) of 1.1 as used in global carbon budget studies such as Manning and Keeling (2006).

5 Conclusions

By continuously measuring atmospheric O_2 and CO_2 concentrations at two heights above a boreal forest in Hyytiälä, Finland, we gained new insights into the diurnal variability of O_2 and CO_2 above a boreal forest, quantified by interpreting their Exchange Ratio (ER). We showed that the signal based on one measurement height of the O_2 and CO_2 concentrations (ER_{atmos}) is

https://doi.org/10.5194/acp-2022-504
Preprint. Discussion started: 18 July 2022


Atmospheric Chemistry and Physics Discussions

not representative for the exchange between the forest and the atmosphere only, but instead includes other processes such as entrainment as well. To derive the ER of the forest (ER_{forest}) specifically, we first determined the surface fluxes above the canopy of O_2 and CO_2 using the vertical gradient between the two measurement heights. We found that the most suitable method to calculate both the O_2 and CO_2 surface fluxes was to calculate the exchange coefficient based on CO_2 gradient calculated using three heights and on the eddy-covariance CO_2 flux. The ER_{forest} signals that resulted from the ratio of the mean O_2 and CO_2 fluxes varied between the daytime (0.92 ± 0.17 mol/mol) and nighttime (1.03 ± 0.05 mol/mol). The different ER_{forest} signals were composed of the ER of respiration (ER_r: 1.03 ± 0.05 mol/mol) and the ER of assimilation (ER_a: 0.96 ± 0.12 mol/mol). With these findings we show improved methods to derive O_2 forest fluxes and to derive the variability in the different ER signals over a representative diurnal cycle. The ER_{forest} signal shows a clear diurnal cycle for this boreal forest and the overall ratio is lower than 1.1 that is used in global carbon budget calculations. Finally, we show that these ER signals can be used to separate Net Ecosystem Exchange (NEE) into Gross Primary Production (GPP) and Total Ecosystem Respiration (TER).

With only a few data sets of continuous measurements of both O_2 and CO_2 concentrations over forests, our data set is of high importance, specifically the availability of measurements at two heights that allow calculation of O_2 and CO_2 fluxes. Our analyses can serve as a starting point for follow up research using coupled land surface-atmosphere models to determine the contributions and partitioning of different processes to ER_{atmos} and ER_{forest} signals. Further understanding of these differences will help to fully make use of the advantages atmospheric O_2 has in unraveling the different components in the carbon cycle.

Data availability. The data in this study are available from https://doi.org/10.18160/SJ3J-PD38.

Author contributions. ITL conducted the measurements and designed measurement the campaign. ITL, ERB, LNTN, PAP and ACM contributed to the design and development of the O_2 and CO_2 measurement setup. LNTN, BAMK, IM and TV contributed to the measurement campaigns. KAPF and ITL analyzed the measurements. KAPF, ITL, WP, JV, HAJM interpreted and discussed the methods and results. KAPF and ITL wrote the manuscript with input from all co-authors.

Competing interests. There are no competing interests.

Acknowledgements. The authors would like to thank Janne Levula (previously worked at Institute for Atmospheric and Earth System Research (INAR) / Physics, Faculty of Science, University of Helsinki, Helsinki, Finland) and Bert Heusinkveld (Meteorology and Air Quality, Wageningen University and Research, Wageningen, the Netherlands) for their help at Hyytiälä during the measurement campaigns, Marcel de Vries (Centre for Isotope Research (CIO), Energy and Sustainability Research Institute Groningen, University of Groningen, Groningen, the Netherlands) for technical support and Charlotte van Leeuwen (previously at Centre for Isotope Research (CIO), Energy and Sustainabil-

https://doi.org/10.5194/acp-2022-504
Preprint. Discussion started: 18 July 2022

Atmospheric Chemistry and Physics Discussions

ity Research Institute Groningen, University of Groningen, Groningen, the Netherlands) for the development of the instrument. This work was supported with funding that ITL received from the Netherlands Organisation for Scientific Research (016.Veni.171.095).

6 Appendix

6.1 Equations to calculate the Exchange Coefficient, K

6.1.1 Observation-based method

The gradient between three points is calculated with the following equation:

$$\overline{\phi}(z) = a \cdot z^2 + b \cdot z + c \tag{9}$$

$$\left(\frac{\partial \overline{\phi}(z)}{\partial z}\right) = 2 \cdot a \cdot z + b \tag{10}$$

Where z is the height above the displacement height (d) (d is taken as: $2/3 \cdot$ canopy height), $\overline{\phi}$ is the average variable where the line is fitted trough and a, b and c are the resulted fitted parameters. When only two vertical measurements are available, the gradient was determined using finite differences.

6.1.2 Theoretical approach

For the MOST method, the following equations were used (Physick and Garratt, 1995):

$$K = \frac{\kappa \cdot z \cdot u_*}{\Phi_H(\frac{z}{L})\phi_{rsl}(\frac{z}{L})} \tag{11}$$

Where κ = 0.4 and is the von Kármán constant, u_* is the friction velocity, Φ_H indicates the stability function and ϕ_{rsl} indicates the contribution of the roughness sublayer (RSL). The Φ_H was calculated with (Dyer, 1974):

$$\Phi_H\left(\frac{z}{L}\right) = \left(1 - 16\frac{z}{L}\right)^{-1/2} \qquad \text{when z/L} < 0 \tag{12}$$

$$\Phi_H\left(\frac{z}{L}\right) = 1 + 5\frac{z}{L} \qquad \text{when z/L} > 0 \tag{13}$$

Where L is the Obukov Lenght, which was based on the following eqation (Dyer, 1974):

$$L = \frac{-u_*^3}{\kappa(\frac{g}{\theta_v})(\overline{w'\theta'_v})} \tag{14}$$

Where θ_v is the virtual potential temperature, $\overline{w'\theta'_v}$ is the virtual surface heat flux and g is the acceleration due to gravity. Because the flux was measured close to the canopy, the roughness surface layer (RSL) could become important. The RSL needs an additional lenght scale (ϕ) and can be calculated with the following equation (de Ridder, 2010):

$$\phi_{HRSL}\left(\frac{z}{z_*}\right) = 1 - e^{-\mu\frac{z}{z_*}} \tag{15}$$

https://doi.org/10.5194/acp-2022-504
Preprint. Discussion started: 18 July 2022


Atmospheric Chemistry and Physics Discussions

Here z_* indicates the height of the RSL above the displacement height and we take that as (2 · canopy height-d) and μ is a constant of 0.95.

By integrating equation 6 with equation 11 for K, we get the following equation that was used for the Integrated method (Physick and Garratt, 1995):

$$\phi(z_2) - \phi(z_1) = \frac{(\overline{w'\phi'})}{\kappa \cdot u_*} \left[ln\left(\frac{z_2}{z_1}\right) - \Psi_H\left(\frac{z_2}{L}\right) + \Psi_H\left(\frac{z_1}{L}\right) + \psi_{RSL}\left(\frac{z}{L}, \frac{z}{z_*}\right) \right] \tag{16}$$

Where Ψ_H are the integrated stability functions for heat and ψ is the integrated function to account for the roughness sublayer (RSL) effectsL. Ψ_H was calculated with (Paulson, 1970):

$$\left.\begin{aligned} \Psi_H\left(\frac{z}{L}\right) &= 2ln\left(\frac{1+x^2}{2}\right) \\ x &= (1-16z/L)^{1/4} \end{aligned}\right\} \quad \text{when z/L} < 0 \tag{17}$$

$$\Psi_H\left(\frac{z}{L}\right) = -5\frac{z}{L} \quad \text{when z/L} > 0 \tag{18}$$

The function of the integrated RSL lenght scale (ψ_{RSL}) was calculated with (de Ridder, 2010):

$$\psi_{RSL}\left(\frac{z}{L}, \frac{z}{z_*}\right) \approx \Phi_H \left[\left(1 + \frac{\nu}{\mu z/z_*}\right) \frac{z}{L} \right] \frac{1}{\lambda} ln\left(1 + \frac{\lambda}{\mu z/z_*}\right) e^{-\mu z/z_*} \tag{19}$$

Where ν and λ are both parameters, taken as 0.5 and 1.5 respectively.

https://doi.org/10.5194/acp-2022-504
Preprint. Discussion started: 18 July 2022

Atmospheric Chemistry and Physics Discussions

References

Angert, A., Yakir, D., Rodeghiero, M., Preisler, Y., Davidson, E. A., and Weiner, T.: Using O_2 to study the relationships between soil CO_2 efflux and soil respiration, Biogeosciences, 12, 2089–2099, https://doi.org/10.5194/bg-12-2089-2015, 2015.

Aubinet, M., Vesala, T., and Papale, D.: Eddy covariance: a practical guide to measurement and data analysis, Springer Science & Business Media, 2012.

Battle, M. O., William Munger, J., Conley, M., Sofen, E., Perry, R., Hart, R., Davis, Z., Scheckman, J., Woogerd, J., Graeter, K., Seekins, S., David, S., and Carpenter, J.: Atmospheric measurements of the terrestrial O_2 : CO_2 exchange ratio of a midlatitude forest, Atmospheric Chemistry and Physics, 19, 8687–8701, https://doi.org/10.5194/acp-19-8687-2019, 2019.

Blaine, T. W., Keeling, R. F., and Paplawsky, W. J.: An improved inlet for precisely measuring the atmospheric Ar/N_2 ratio, Atmospheric Chemistry and Physics, 6, 1181–1184, https://doi.org/10.5194/acp-6-1181-2006, 2006.

Bloom, A. J., Caldwell, R. M., Finazzo, J., Warner, R. L., and Weissbart, J.: Oxygen and Carbon Dioxide Fluxes from Barley Shoots Depend on Nitrate Assimilation, Plant Physiology, 91, 352–356, https://doi.org/10.1104/pp.91.1.352, 1989.

Bloom, A. J., Rubio Asensio, J. S., Randall, L., Rachmilevitch, S., Cousins, A. B., and Carlisle, E. A.: CO_2 enrichment inhibits shoot nitrate assimilation in C3 but not C4 plants and slows growth under nitrate in C3 plants, Ecology, 93, 355–367, https://doi.org/10.1890/11-0485.1, 2012.

Bolinius, D. J., Jahnke, A., and MacLeod, M.: Comparison of eddy covariance and modified Bowen ratio methods for measuring gas fluxes and implications for measuring fluxes of persistent organic pollutants, Atmospheric Chemistry and Physics, 16, 5315–5322, https://doi.org/10.5194/acp-16-5315-2016, 2016.

Bonan, G. B.: Forests and climate change: forcings, feedbacks, and the climate benefits of forests, science, 320, 1444–1449, 2008.

Brown, J., Shapkalijevski, M., Krol, M., Karl, T., Ouwersloot, H., Moene, A., Patton, E., and Vilà-Guerau de Arellano, J.: Ozone exchange within and above an irrigated Californian orchard, Tellus B: Chemical and Physical Meteorology, 72, 1–17, 2020.

Buurman, P. and Jongmans, A.: Podzolisation and soil organic matter dynamics, Geoderma, 125, 71–83, 2005.

Carbon Portal ICOS RI: STILT station characterization for Hyytiälä at 17m, https://hdl.handle.net/11676/sbjAXeKbI09FqHDtFNqf6oVc, 2022.

Casso-Torralba, P., de Arellano, J. V. G., Bosveld, F., Soler, M. R., Vermeulen, A., Werner, C., and Moors, E.: Diurnal and vertical variability of the sensible heat and carbon dioxide budgets in the atmospheric surface layer, Journal of Geophysical Research Atmospheres, 113, https://doi.org/10.1029/2007JD009583, 2008.

Crotwell, A., Lee, H., and Steinbacher, M.: 20th WMO/IAEA Meeting on Carbon Dioxide, Other Greenhouse Gases and Related Measurement Techniques (GGMT-2019), Tech. Rep. 255, 2020.

de Ridder, K.: Bulk transfer relations for the roughness sublayer, Boundary-Layer Meteorology, 134, 257–267, https://doi.org/10.1007/s10546-009-9450-y, 2010.

Dyer, A.: A review of flux-profile relationships, Boundary-Layer Meteorology, 7, 363–372, 1974.

Friedlingstein, P., Jones, M. W., O'Sullivan, M., Andrew, R. M., Bakker, D. C. E., Hauck, J., Le Quéré, C., Peters, G. P., Peters, W., Pongratz, J., Sitch, S., Canadell, J. G., Ciais, P., Jackson, R. B., Alin, S. R., Anthoni, P., Bates, N. R., Becker, M., Bellouin, N., Bopp, L., Chau, T. T. T., Chevallier, F., Chini, L. P., Cronin, M., Currie, K. I., Decharme, B., Djeutchouang, L. M., Dou, X., Evans, W., Feely, R. A., Feng, L., Gasser, T., Gilfillan, D., Gkritzalis, T., Grassi, G., Gregor, L., Gruber, N., Gürses, O., Harris, I., Houghton, R. A., Hurtt, G. C., Iida, Y., Ilyina, T., Luijkx, I. T., Jain, A., Jones, S. D., Kato, E., Kennedy, D., Klein Goldewijk, K., Knauer, J., Korsbakken, J. I., Körtzinger,

https://doi.org/10.5194/acp-2022-504
Preprint. Discussion started: 18 July 2022

A., Landschützer, P., Lauvset, S. K., Lefèvre, N., Lienert, S., Liu, J., Marland, G., McGuire, P. C., Melton, J. R., Munro, D. R., Nabel, J. E. M. S., Nakaoka, S.-I., Niwa, Y., Ono, T., Pierrot, D., Poulter, B., Rehder, G., Resplandy, L., Robertson, E., Rödenbeck, C., Rosan, T. M., Schwinger, J., Schwingshackl, C., Séférian, R., Sutton, A. J., Sweeney, C., Tanhua, T., Tans, P. P., Tian, H., Tilbrook, B., Tubiello, F., van der Werf, G. R., Vuichard, N., Wada, C., Wanninkhof, R., Watson, A. J., Willis, D., Wiltshire, A. J., Yuan, W., Yue, C., Yue, X., Zaehle, S., and Zeng, J.: Global Carbon Budget 2021, Earth System Science Data, 14, 1917–2005, https://doi.org/10.5194/essd-14-1917-2022, 2022.

Gallagher, M. E., Liljestrand, F. L., Hockaday, W. C., and Masiello, C. A.: Plant species, not climate, controls aboveground biomass O_2:CO_2 exchange ratios in deciduous and coniferous ecosystems, Journal of Geophysical Research: Biogeosciences, 122, 2314–2324, https://doi.org/10.1002/2017JG003847, 2017.

Hari, P., Nikinmaa, E., Pohja, T., Siivola, E., Bäck, J., Vesala, T., and Kulmala, M.: Station for measuring ecosystem-atmosphere relations: SMEAR, in: Physical and physiological forest ecology, pp. 471–487, Springer, 2013.

Ishidoya, S., Murayama, S., Takamura, C., Kondo, H., Saigusa, N., Goto, D., Morimoto, S., Aoki, N., Aoki, S., and Nakazawa, T.: O_2:CO_2 exchange ratios observed in a cool temperate deciduous forest ecosystem of central Japan , Tellus B: Chemical and Physical Meteorology, 65, 21 120, https://doi.org/10.3402/tellusb.v65i0.21120, 2013.

Ishidoya, S., Murayama, S., Kondo, H., Saigusa, N., Kishimoto-Mo, A. W., and Yamamoto, S.: Observation of O_2:CO_2 exchange ratio for net turbulent fluxes and its application to forest carbon cycles, Ecological Research, 30, 225–234, https://doi.org/10.1007/s11284-014-1241-3, 2015.

Jürgensen, J., Muhr, J., and Knohl, A.: Variations of the Oxidative Ratio across Ecosystem Components and Seasons in a Managed Temperate Beech Forest (Leinefelde, Germany), Forests, 12, 1693, 2021.

Keeling, R.: Development of an Interferometric Oxygen Analyzer for Precise Measurement of the Atmospheric O_2 Mole Fraction., Ph.D. thesis, Harvard University, 1988.

Keeling, R., Najjar, R., Bender, M., and Tans, P.: What atmospheric oxygen measurements can tell us about the global carbon-cycle, Global Biogeochemical Cycles, 7, 37–67, https://doi.org/10.1029/92GB02733, 1993.

Keeling, R. F. and Manning, A. C.: Studies of Recent Changes in Atmospheric O_2 Content, vol. 5, Elsevier Ltd., 2 edn., https://doi.org/10.1016/B978-0-08-095975-7.00420-4, 2014.

Keeling, R. F., Manning, A. C., McEvoy, E. M., and Shertz, S. R.: Methods for measuring changes in atmospheric O_2 concentration and their application in southern hemisphere air, Journal of Geophysical Research: Atmospheres, 103, 3381–3397, 1998.

Keeling, R. F., Manning, A. C., Paplawsky, W. J., and Cox, A. C.: On the long-term stability of reference gases for atmospheric O2/N2 and CO_2 measurements, Tellus B: Chemical and Physical Meteorology, 59, 3–14, https://doi.org/10.1111/j.1600-0889.2006.00196.x, 2007.

Kooijmans, L. M., Cho, A., Ma, J., Kaushik, A., Haynes, K. D., Baker, I., Luijkx, I. T., Groenink, M., Peters, W., Miller, J. B., et al.: Evaluation of carbonyl sulfide biosphere exchange in the Simple Biosphere Model (SiB4), Biogeosciences, 18, 6547–6565, 2021.

Koren, G., Schneider, L., van der Velde, I. R., van Schaik, E., Gromov, S. S., Adnew, G. A., Mrozek Martino, D. J., Hofmann, M. E., Liang, M.-C., Mahata, S., et al.: Global 3-D Simulations of the Triple Oxygen Isotope Signature Δ17O in Atmospheric CO_2, Journal of Geophysical Research: Atmospheres, 124, 8808–8836, 2019.

Korhonen, J., Pihlatie, M., Pumpanen, J., Aaltonen, H., Hari, P., Levula, J., Kieloaho, A.-J., Nikinmaa, E., Vesala, T., and Ilvesniemi, H.: Nitrogen balance of a boreal Scots pine forest, Biogeosciences, 10, 1083–1095, 2013.

https://doi.org/10.5194/acp-2022-504
Preprint. Discussion started: 18 July 2022

Kozlova, E. A. and Manning, A. C.: Methodology and calibration for continuous measurements of biogeochemical trace gas and O_2 concentrations from a 300-m tall tower in central Siberia, Atmospheric Measurement Techniques, 2, 205–220, https://doi.org/10.5194/amt-2-205-2009, 2009.

Kulmala, L., Pumpanen, J., Kolari, P., Dengel, S., Berninger, F., Köster, K., Matkala, L., Vanhatalo, A., Vesala, T., and Bäck, J.: Inter-and intra-annual dynamics of photosynthesis differ between forest floor vegetation and tree canopy in a subarctic Scots pine stand, Agricultural and Forest Meteorology, 271, 1–11, 2019.

Manning, A. C.: Temporal variability of atmospheric oxygen from both continuous measurements and a flask sampling network: Tools for studying the global carbon cycle, University of California, San Diego, 2001.

Manning, A. C. and Keeling, R. F.: Global oceanic and land biotic carbon sinks from the scripps atmospheric oxygen flask sampling network, Tellus, Series B: Chemical and Physical Meteorology, 58, 95–116, https://doi.org/10.1111/j.1600-0889.2006.00175.x, 2006.

Mayer, J. C., Bargsten, A., Rummel, U., Meixner, F. X., and Foken, T.: Distributed Modified Bowen Ratio method for surface layer fluxes of reactive and non-reactive trace gases, Agricultural and Forest Meteorology, 151, 655–668, https://doi.org/10.1016/j.agrformet.2010.10.001, 2011.

Meyers, T. P., Hall, M. E., Lindberg, S. E., and Kim, K.: Use of the modified Bowen-ratio technique to measure fluxes of trace gases, Atmospheric Environment, 30, 3321–3329, 1996.

Nguyen, L. N., Meijer, H. A., van Leeuwen, C., Kers, B. A., Scheeren, H. A., Jones, A. E., Brough, N., Barningham, T., Pickers, P. A., Manning, A. C., et al.: Two decades of flask observations of atmospheric δ (O_2/N_2), CO 2, and APO at stations Lutjewad (the Netherlands) and Mace Head (Ireland), and 3 years from Halley station (Antarctica), Earth System Science Data, 14, 991–1014, 2022.

Paulson, C. A.: The mathematical representation of wind speed and temperature profiles in the unstable atmospheric surface layer, Journal of Applied Meteorology and Climatology, 9, 857–861, 1970.

Peters, W., van der Velde, I. R., Van Schaik, E., Miller, J. B., Ciais, P., Duarte, H. F., van der Laan-Luijkx, I. T., van der Molen, M. K., Scholze, M., Schaefer, K., et al.: Increased water-use efficiency and reduced CO_2 uptake by plants during droughts at a continental scale, Nature geoscience, 11, 744–748, 2018.

Peters, W., Bastos, A., Ciais, P., and Vermeulen, A.: A historical, geographical and ecological perspective on the 2018 European summer drought, 2020.

Physick, W. and Garratt, J.: Incorporation of a high-roughness lower boundary into a mesoscale model for studies of dry deposition over complex terrain, Boundary-Layer Meteorology, 74, 55–71, 1995.

Pickers, P. A., Manning, A. C., Sturges, W. T., Le Quéré, C., Mikaloff Fletcher, S. E., Wilson, P. A., and Etchells, A. J.: In situ measurements of atmospheric O_2 and CO_2 reveal an unexpected O2 signal over the tropical Atlantic Ocean, Global Biogeochemical Cycles, 31, 1289–1305, 2017.

Pickers, P. A., Manning, A. C., Le Quéré, C., Forster, G. L., Luijkx, I. T., Gerbig, C., Fleming, L. S., and Sturges, W. T.: Novel quantification of regional fossil fuel CO_2 reductions during COVID-19 lockdowns using atmospheric oxygen measurements, Science advances, 8, eabl9250, 2022.

Popa, M. E., Gloor, M., Manning, A. C., Jordan, A., Schultz, U., Haensel, F., Seifert, T., and Heimann, M.: Measurements of greenhouse gases and related tracers at Bialystok tall tower station in Poland, Atmospheric Measurement Techniques, 3, 407–427, https://doi.org/10.5194/amt-3-407-2010, 2010.

https://doi.org/10.5194/acp-2022-504
Preprint. Discussion started: 18 July 2022

Atmospheric Chemistry and Physics Discussions

Randerson, J. T., Masiello, C. A., Still, C. J., Rahn, T., Poorter, H., and Field, C. B.: Is carbon within the global terrestrial biosphere becoming more oxidized? Implications for trends in atmospheric O_2 , Global Change Biology, 12, 260–271, https://doi.org/10.1111/j.1365-2486.2006.01099.x, 2006.

Reichstein, M., Falge, E., Baldocchi, D., Papale, D., Aubinet, M., Berbigier, P., Bernhofer, C., Buchmann, N., Gilmanov, T., Granier, A., et al.: On the separation of net ecosystem exchange into assimilation and ecosystem respiration: review and improved algorithm, Global change biology, 11, 1424–1439, 2005.

Rödenbeck, C., Le Quéré, C., Heimann, M., and Keeling, R. F.: Interannual variability in oceanic biogeochemical processes inferred by inversion of atmospheric O_2/N_2 and CO_2 data, Tellus, Series B: Chemical and Physical Meteorology, 60 B, 685–705, https://doi.org/10.1111/j.1600-0889.2008.00375.x, 2008.

Rousseeuw, P. J. and Verboven, S.: Robust estimation in very small samples, Computational Statistics & Data Analysis, 40, 741–758, 2002.

Seibt, U., Brand, W. A., Heimann, M., Lloyd, J., Severinghaus, J. P., and Wingate, L.: Observations of O_2 : CO_2 exchange ratios during ecosystem gas exchange, Global Biogeochemical Cycles, 18, 1–18, https://doi.org/10.1029/2004GB002242, 2004.

Severinghaus, J. P.: Studies of the Terrestrial O_2 and Carbon Cycles in Sand Dune Gases and in Biosphere, Ph.D. thesis, Columbia University, https://doi.org/10.2172/477735, 1995.

Stephens, B. B., Keeling, R. F., Heimann, M., Six, K. D., Murnane, R., and Caldeira, K.: Testing global ocean carbon cycle models using measurements of atmospheric O_2 and CO_2 concentration, Global Biogeochemical Cycles, 12, 213–230, https://doi.org/10.1029/97GB03500, 1998.

Stephens, B. B., Bakwin, P. S., Tans, P. P., Teclaw, R. M., and Baumann, D. D.: Application of a differential fuel-cell analyzer for measuring atmospheric oxygen variations, Journal of Atmospheric and Oceanic Technology, 24, 82–94, https://doi.org/10.1175/JTECH1959.1, 2007.

Stull, R. B.: An introduction to boundary layer meteorology, vol. 13, Springer Science & Business Media, 1988.

Tohjima, Y., Machida, T., Watai, T., Akama, I., Amari, T., and Moriwaki, Y.: Preparation of gravimetric standards for measurements of atmospheric oxygen and reevaluation of atmospheric oxygen concentration., Journal of Geophysical Research–Atmospheres, 110, D11 302, https://doi.org/10.1029/2004JD005595, 2005.

Tohjima, Y., Mukai, H., Machida, T., Hoshina, Y., and Nakaoka, S.-I.: Global carbon budgets estimated from atmospheric $\delta O_2/N_2$ and CO_2 observations in the western Pacific region over a 15-year period, Atmospheric Chemistry and Physics, 19, 9269–9285, 2019.

van der Laan, S., van der Laan-Luijkx, I. T., Rödenbeck, C., Varlagin, A., Shironya, I., Neubert, R. E., Ramonet, M., and Meijer, H. A.: Atmospheric CO_2, $\delta(O_2/N_2)$, APO and oxidative ratios from aircraft flask samples over Fyodorovskoye, Western Russia, Atmospheric Environment, 97, 174–181, https://doi.org/10.1016/j.atmosenv.2014.08.022, 2014.

van der Laan-Luijkx, I. T., Neubert, R. E., van der Laan, S., and Meijer, H. A.: Continuous measurements of atmospheric oxygen and carbon dioxide on a North Sea gas platform, Atmospheric Measurement Techniques, 3, 113–125, https://doi.org/10.5194/amt-3-113-2010, 2010.

van Leeuwen, C. and Meijer, H. A.: Detection of CO_2 leaks from carbon capture and storage sites with combined atmospheric CO_2 and O_2 measurements, International Journal of Greenhouse Gas Control, 41, 194–209, https://doi.org/10.1016/j.ijggc.2015.07.019, 2015.

Vilà-Guerau de Arellano, J., Gioli, B., Miglietta, F., Jonker, H. J., Baltink, H. K., Hutjes, R. W., and Holtslag, A. A.: Entrainment process of carbon dioxide in the atmospheric boundary layer, Journal of Geophysical Research Atmospheres, 109, 1–16, https://doi.org/10.1029/2004JD004725, 2004.

Whelan, M. E., Lennartz, S. T., Gimeno, T. E., Wehr, R., Wohlfahrt, G., Wang, Y., Kooijmans, L. M. J., Hilton, T. W., Belviso, S., Peylin, P., Commane, R., Sun, W., Chen, H., Kuai, L., Mammarella, I., Maseyk, K., Berkelhammer, M., Li, K.-F., Yakir, D., Zumkehr, A., Katayama, Y., Ogée, J., Spielmann, F. M., Kitz, F., Rastogi, B., Kesselmeier, J., Marshall, J., Erkkilä, K.-M., Wingate, L., Meredith, L. K., He, W.,

https://doi.org/10.5194/acp-2022-504
Preprint. Discussion started: 18 July 2022

Bunk, R., Launois, T., Vesala, T., Schmidt, J. A., Fichot, C. G., Seibt, U., Saleska, S., Saltzman, E. S., Montzka, S. A., Berry, J. A., and Campbell, J. E.: Reviews and syntheses: Carbonyl sulfide as a multi-scale tracer for carbon and water cycles, Biogeosciences, 15, 3625–3657, https://doi.org/10.5194/bg-15-3625-2018, 2018.

Wolf, A., Saliendra, N., Akshalov, K., Johnson, D. A., and Laca, E.: Effects of different eddy covariance correction schemes on energy balance closure and comparisons with the modified Bowen ratio system, Agricultural and Forest Meteorology, 148, 942–952, https://doi.org/10.1016/j.agrformet.2008.01.005, 2008.

Worrall, F., Clay, G. D., Masiello, C. A., and Mynheer, G.: Estimating the oxidative ratio of the global terrestrial biosphere carbon, Biogeochemistry, 115, 23–32, https://doi.org/10.1007/s10533-013-9877-6, 2013.